

Kinetic theory of granular particles immersed in a molecular gas

RUBÉN GÓMEZ GONZÁLEZ¹ and VICENTE GARZÓ²

¹Departamento de Física, Universidad de Extremadura, Avda. de Elvas s/n, 06006 Badajoz (Spain)

² Departamento de Física, Instituto Universitario de Computación Científica Avanzada (ICCAEx), Universidad de Extremadura, Avda. de Elvas s/n, 06006 Badajoz (Spain).

(Received xx; revised xx; accepted xx)

The transport coefficients of a dilute gas of inelastic hard spheres immersed in a molecular gas are determined. We assume that the number density of the granular gas is much smaller than that of the surrounding molecular gas, so that the latter is not affected by the presence of solid particles. In this situation, the molecular gas may be treated as a thermostat (or bath) of elastic hard spheres at a fixed temperature. This system (granular gas thermostated by a bath of elastic hard spheres) can be considered as a reliable model for describing the dynamic properties of particle-laden suspensions. The Boltzmann kinetic equation is the starting point of the present work. First step is to characterise the reference state in the perturbation scheme, namely the homogeneous state. Theoretical results for the *granular* temperature and kurtosis obtained in the homogeneous steady state are compared against Monte Carlo simulations showing a good agreement. Then, the Chapman–Enskog method is employed to solve the Boltzmann equation to first order in spatial gradients. As expected, the Navier–Stokes–Fourier transport coefficients of the granular gas are given in terms of the solutions of a coupled set of linear integral equations which are approximately solved by considering the leading terms in a Sonine polynomial expansion. Our results show that the dependence of the transport coefficients on the coefficient of restitution is quite different from that found when the influence of the interstitial molecular gas is neglected (dry granular gas). When the granular particles are much more heavier than the gas particles (Brownian limit) the expressions of the transport coefficients are consistent with those previously derived from the Fokker–Planck equation. Finally, as an application of the theory, a linear stability analysis of the homogeneous steady state is performed showing this state is always linearly stable.

1. Introduction

A challenging problem in statistical physics is the understanding of multiphase flows, namely, the flow of solid particles in two or more thermodynamic phases. Needless to say, these type of flows occur in many industrial settings (such as circulating fluidised beds) and can also affect our daily lives due to the fact that the comprehension of them may ensure vital needs of humans such as clean air and water (Subramaniam 2020). Among the different types of multiphase flows, a particularly interesting set corresponds to the so-called particle-laden suspensions in which small, immiscible and typically dilute particles are immersed in a carrier fluid (for instance, fine aerosol particles in air). The dynamics of gas-solid flows is rich and extraordinarily complex (Gidaspow 1994; Jackson 2000; Koch & Hill 2001; Fox 2012; Tenneti & Subramaniam 2014; Fullmer & Hrenya 2017; Lattanzi *et al.* 2020) so their understanding poses a great challenge. Even the study of granular

flows in which the effect of interstitial fluid is neglected (Campbell 1990; Goldhirsch 2003; Rao & Nott 2008; Brilliantov & Pöschel 2004; Garzó 2019) entails enormous difficulties.

In the case that the particle-laden suspensions are dominated by collisions (Subramaniam 2020), the extension of the classical kinetic theory of gases (Chapman & Cowling 1970; Ferziger & Kaper 1972; Résibois & de Leener 1977) to gas-solid systems for relatively massive particles (high Stokes numbers) can be considered as an appropriate tool to model these systems. In this context and assuming nearly instantaneous collisions, the influence of gas-phase effects on the dynamics of solid particles is usually incorporated in the starting kinetic equation in an effective way via a fluid-solid interaction force (Koch 1990; Gidaspow 1994; Jackson 2000). Some models for gas-solid suspensions (Louge *et al.* 1991; Tsao & Koch 1995; Sangani *et al.* 1996; Wylie *et al.* 2009; Parmentier & Simonin 2012; Heussinger 2013; Wang *et al.* 2014; Saha & Alam 2017; Alam *et al.* 2019; Saha & Alam 2020) only consider the Stokes linear drag law for gas-solid interactions. Other models (Garzó *et al.* 2012) include also an additional Langevin-type stochastic term. In this case, based on the results obtained in direct numerical simulations (DNS), the impact of the viscous gas on solid particles in high-velocity—but low-Reynold numbers—gas-solid flows is by means of a force constituted by three different terms: (i) a term proportional to the difference between the mean flow velocities of both phases, (ii) a drag force term proportional to the particle velocity, and (iii) a stochastic Langevin-like term taking into account the effects of neighbouring particles. While the second term mimics the dissipation of energy due to the friction of grains on the viscous gas, the third term models the energy gained by the solid particles due to their interaction with the particles of the interstitial gas.

For small Knudsen numbers, the above suspension model (Garzó *et al.* 2012) has been solved by means of the Chapman–Enskog method (Chapman & Cowling 1970) adapted to dissipative dynamics. Explicit expressions for the Navier–Stokes–Fourier transport coefficients have been obtained in terms of the coefficient of restitution and the parameters of the suspension model (Garzó *et al.* 2012; Gómez González & Garzó 2019). The knowledge of the forms of the transport coefficients has allowed to assess not only the impact of inelasticity on them [which was already analysed in the case of dry granular fluids (Brey *et al.* 1998; Garzó & Dufty 1999)] but also the influence of the interstitial gas on the momentum and heat transport. Beyond the Navier–Stokes domain, this type of suspension models have been also considered to compute the rheological properties in sheared gas-solid suspensions [see for instance, Tsao & Koch (1995); Sangani *et al.* (1996); Parmentier & Simonin (2012); Heussinger (2013); Seto *et al.* (2013); Kawasaki *et al.* (2014); Chamorro *et al.* (2015); Saha & Alam (2017); Hayakawa *et al.* (2017); Alam *et al.* (2019); Hayakawa & Takada (2019); Saha & Alam (2020); Gómez González & Garzó (2020); Takada *et al.* (2020)].

The quantitative and qualitative accuracy of the (approximate) analytical results derived from the kinetic-theory two-fluid model (Garzó *et al.* 2012) have been confronted against computer simulations in several problems. In particular, the critical length for the onset of velocity vortices in the homogeneous cooling state of gas-solid flows obtained from a linear stability analysis presents an acceptable agreement with molecular dynamics (MD) simulations carried out for strong inelasticity (Garzó *et al.* 2016). Simulations using a computational fluid dynamics (CFD) solver (Capecelatro & Desjardins 2013; Capecelatro *et al.* 2015) of Radl & Sundaresan (2014) have shown a good agreement in the mean slip velocity with the kinetic-theory predictions (Fullmer & Hrenya 2016). On the other hand, kinetic theory has been also assessed for describing clustering instabilities in sedimenting fluid-solid systems; good agreement is found at high solid-to-fluid density ratios although the agreement is weaker for intermediate and low density ratios (Fullmer

et al. 2017). In the case of non-Newtonian flows, the theoretical results (Saha & Alam 2017; Alam *et al.* 2019; Saha & Alam 2020) derived from the Stokes drag model for the ignited-quenched transition and the rheology of a sheared gas-solid suspension have been shown to compare very well with computer simulations. Regarding the Langevin-like model (Garzó *et al.* 2012), the rheological properties of a moderately dense inertial suspension computed by a simpler version of this model exhibit a quantitative good agreement with MD simulations in the high-density region (Takada *et al.* 2020). In addition, the extension to binary mixtures of this suspension model has been tested against Monte Carlo data and MD simulations for both time-dependent and steady homogeneous states with an excellent agreement (Khalil & Garzó 2014; Gómez González *et al.* 2020; Gómez González & Garzó 2021).

In spite of the reliability of the generalised Langevin and Stokes drag models for capturing in an effective way the impact of gas phase on grains, it would be desirable to propose a suspension model that considers the real collisions between solid and gas particles. In the context of kinetic theory and as already mentioned in previous works (Gómez González *et al.* 2020), a possibility would be to describe gas-solid flows in terms of a set of two coupled kinetic equations for the one-particle velocity distribution functions of the solid and gas phases. Nevertheless, the determination of the transport coefficients of the solid particles starting from the above suspension model is a very intricate problem. A possible way of overcoming the difficulties inherent to the description of gas-solid flows when one attempts to involve the different types of collisions is to assume that the properties of the gas phase are unaffected by the presence of solid particles. In fact, although sometimes not explicitly stated, this is one of the overarching assumptions in most of the suspension models reported in the granular literature. This assumption can be clearly justified in the case of particle-laden suspensions where the granular particles (or “granular gas”) are sufficiently rarefied (dilute particles) and hence, the properties of the interstitial fluid can be supposed to be constant. This means that the background gas can be treated as a *thermostat* at a constant temperature T_g .

Under these conditions and inspired in a paper of Biben *et al.* (2002), we propose here the following suspension model. We consider a set of *granular* particles immersed in a bath of elastic particles (*molecular* gas) at equilibrium at a certain temperature T_g . While the collisions between granular particles are *inelastic* (and characterised by a constant coefficient of normal restitution α), the collisions between the granular and gas particles are considered to be elastic. In the homogeneous steady state, the energy lost by the solid particles due to their collisions among themselves is exactly compensated for by the energy gained by the grains due to their elastic collisions with particles of the molecular gas. In other words, the gas of *inelastic* hard spheres (granular gas) is thermostated by a bath of *elastic* hard spheres. The dynamic properties of this system in homogeneous steady states were studied years ago independently by Biben *et al.* (2002) and Santos (2003). Our goal here is going beyond the homogeneous state and determine the transport coefficients of the granular gas immersed in the molecular gas when the magnitude of the spatial gradients is small (Navier–Stokes domain).

It is quite apparent that this suspension model (granular particles plus molecular gas) can be seen as a binary mixture in which the concentration of one of the species (tracer species or granular particles) is much smaller than the other one (excess species or molecular gas). In these conditions, it is reasonable to assume that the state of the background gas (excess species) is not perturbed by the presence of the tracer species (granular particles). In addition, although the density of grains is very small, we will take into account not only the collisions between solid and gas particles, but also the grain-grain collisions in the kinetic equation of the one-particle distribution function $f(\mathbf{r}, \mathbf{v}; t)$

of solid particles. In spite of the simplicity of the model, it can be considered sufficiently robust since it retains most of the basic features of gas-solid flows such as the competition between the different spatial and time scales. As an added value and in contrast to the usual suspension models reported in the literature (Koch 1990; Gidaspow 1994; Jackson 2000), the model incorporates a new parameter: the ratio between the mass m of the granular particles and the mass m_g of the particles of the molecular gas.

As mentioned before, the main goal of the paper is to determine the Navier–Stokes–Fourier transport coefficients of the granular particles thermostated by a bath of elastic hard spheres. For a low-density granular gas, the distribution function $f(\mathbf{r}, \mathbf{v}; t)$ verifies the Boltzmann kinetic equation. More specifically, since granular particles collides among themselves and with particles of the molecular gas, the time evolution of the distribution f involves the Boltzmann $J[f, f]$ and Boltzmann–Lorentz $J_g[f, f_g]$ collisions operators. Here, f_g is the one-particle distribution function of the molecular gas. While the (nonlinear) collision operator J accounts for the rate of change of f due to inelastic collisions, the (linear) operator J_g accounts for the rate of change of f due to the elastic collisions between grains and gas particles. Interestingly, in the Brownian limiting case ($m \gg m_g$), the Boltzmann–Lorentz operator reduces to the Fokker–Planck operator so that, the results derived here reduce to those previously obtained by Gómez González & Garzó (2019) in this limiting case.

As in previous works (Garzó *et al.* 2013; Gómez González & Garzó 2019), the transport coefficients are determined by solving the Boltzmann equation by the generalisation of the conventional Chapman–Enskog expansion (Chapman & Cowling 1970) to inelastic gases (Brilliantov & Pöschel 2004; Garzó 2019). An important point in the perturbation method is the choice of the reference base state (zeroth-order approximation $f^{(0)}$). In the case of dry granular gases (no gas phase) and in the absence of spatial gradients, the solution $f^{(0)}(\mathbf{r}, \mathbf{v}; t)$ to the Boltzmann equation is the *local* version of the so-called homogeneous cooling state (HCS). On the other hand, in the case of granular suspensions, although one is interested in computing transport in steady conditions, the presence of the background molecular gas may induce a *local* energy unbalance between the energy lost due to inelastic collisions and the energy transfer via elastic collisions. This leads in general to a non-stationary zeroth-order distribution $f^{(0)}$. Thus, as already did in previous calculations (Garzó *et al.* 2013; Gómez González & Garzó 2019), we have to consider first the time-dependent distribution $f^{(0)}(\mathbf{r}, \mathbf{v}; t)$ in order to arrive to the linear integral equations obeying the Navier–Stokes–Fourier transport coefficients. Then, to get explicit forms for the transport coefficients, the above integral equations are (approximately) solved under steady state conditions.

The plan of the paper is as follows. The Boltzmann kinetic equation for a granular gas immersed in a molecular gas is presented in section 2 along with the corresponding balance equations for the densities of mass, momentum, and energy. The Brownian limit ($m/m_g \rightarrow \infty$) is also considered; it is shown that the Boltzmann–Lorentz operator $J_g[\mathbf{v}|f, f_g]$ reduces in this limiting case to the Fokker–Planck operator (Résibois & de Leener 1977; McLennan 1989), which is the basis of the Langevin-like suspension model (Garzó *et al.* 2012). Section 3 is devoted to the study of the homogeneous steady state (HSS). Although the HSS was already analysed by Santos (2003) for a three-dimensional system ($d = 3$), we revisit here this study by extending the analysis to an arbitrary number of dimensions d . As usual, the first-Sonine approximation to the velocity distribution $f(\mathbf{v})$ is considered to determine the temperature ratio T/T_g and the fourth cumulant (or kurtosis) a_2 in terms of the parameter space of the system: the dimensionality d , the coefficient of restitution α , the mass ratio m/m_g , the volume fraction ϕ , and the (reduced) background temperature T_g^* . In the above Sonine solution,

only linear terms in a_2 are considered. The theoretical results are compared against Monte Carlo simulations for $d = 3$, $\phi = 0.001$, $T_g^* = 1000$, and different values of the mass ratio. The comparison shows in general an excellent agreement for the temperature ratio; some small quantitative discrepancies are found for a_2 in the case $m/m_g = 1$.

Section 4 addresses the application of the Chapman–Enskog-like expansion (Chapman & Cowling 1970) to the Boltzmann kinetic equation. Since the system is slightly disturbed from the HSS, the expansion is around the *local* version of the homogeneous state. However, as said before, for general small deviations from the homogeneous state the zeroth-order (reference) distribution function $f^{(0)}(\mathbf{r}, \mathbf{v}; t)$ is a time-dependent distribution. As usual for elastic collisions (Chapman & Cowling 1970; Ferziger & Kaper 1972), the Navier–Stokes–Fourier transport coefficients are in given in terms of the solutions of a set of coupled linear integral equations. On the other hand, due to the mathematical difficulties involved in the time-dependent problem, as in previous works (Garzó *et al.* 2013; Gómez González & Garzó 2019) the general results are restricted to steady-state conditions, namely, when the constraint $\zeta^{(0)} + \zeta_g^{(0)} = 0$ holds at any point of the system. Here, $\zeta^{(0)}$ and $\zeta_g^{(0)}$ are the zeroth-order contributions to the partial production rates due to solid-solid and solid-gas collisions, respectively. In the steady state, explicit expressions of the Navier–Stokes–Fourier transport coefficients are obtained in section 5 by considering the leading terms in a Sonine polynomial expansion. As in the case of the temperature ratio and the kurtosis, in dimensionless form, the transport coefficients are provided in terms of α , m/m_g , ϕ , and T_g^* . An interesting result is that the expressions of the transport coefficients reduce to those previously obtained by Gómez González & Garzó (2019) in the Brownian limit ($m/m_g \rightarrow \infty$). As an application of the results reported in section 5, a linear stability analysis of the HSS is carried out in section 6. Analogously to the analysis performed in the Brownian limit (Gómez González & Garzó 2019), the present analysis shows that the HSS is linearly stable regardless the value of the mass ratio m/m_g . The paper is ended in section 7 with a brief summary of the results reported here.

2. Boltzmann kinetic equation for a granular gas surrounded by a molecular gas

We consider a gas of inelastic hard disks ($d = 2$) or spheres ($d = 3$) of mass m and diameter σ . The spheres are assumed to be perfectly smooth so that, collisions between pairs are characterised by a (positive) constant coefficient of normal restitution $\alpha \leq 1$. When $\alpha = 1$ ($\alpha < 1$), the collisions are elastic (inelastic). The granular gas is immersed in a molecular gas constituted by hard disks or spheres of mass m_g and diameter σ_g . Collisions between granular particles and gas molecules are considered to be *elastic*. As discussed in section 1, we are interested here in describing a situation where the granular gas is sufficiently rarefied (the number density of granular particles is much smaller than that of the molecular gas) so that, the state of the molecular gas is not affected by the presence of solid (grains) particles. In this sense, the background (molecular) gas may be treated as a *thermostat*, which is at equilibrium at the temperature T_g . Thus, the velocity distribution function f_g of the molecular gas is the Maxwell–Boltzmann distribution:

$$f_g(\mathbf{V}_g) = n_g \left(\frac{m_g}{2\pi T_g} \right)^{d/2} \exp \left(- \frac{m_g V_g^2}{2T_g} \right), \quad (2.1)$$

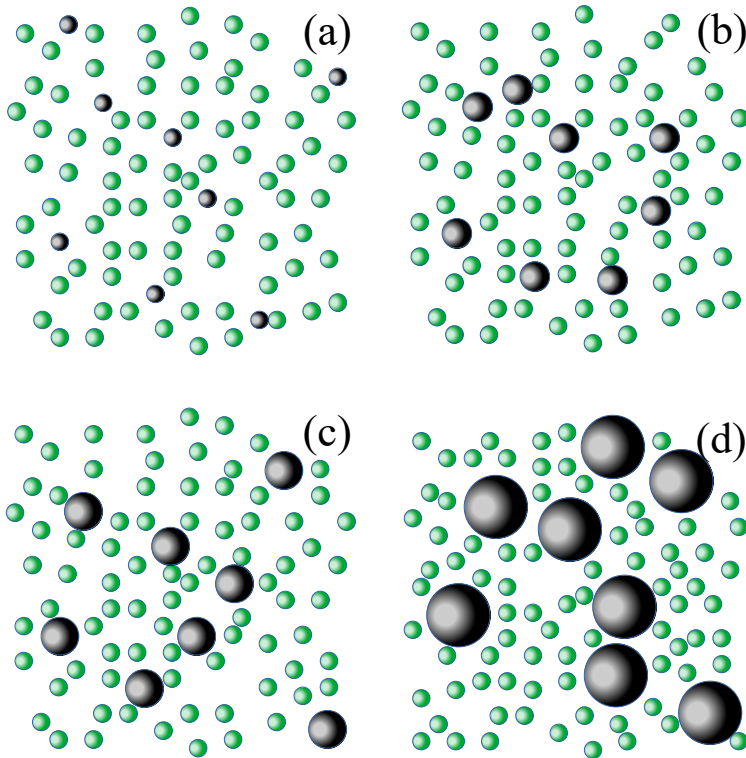


FIGURE 1. Schematic plot of granular particles immersed in a molecular gas. Four different mass ratios are represented: $m/m_g = 1$ (a), $m/m_g = 5$ (b), $m/m_g = 10$ (c), and $m/m_g = 50$ (d). Particles density m/σ^3 is constant in all the panels. Number density ratio is kept fixed to $n_g/n = 10$.

where n_g is the number density of the molecular gas, $\mathbf{V}_g = \mathbf{v} - \mathbf{U}_g$, and \mathbf{U}_g is the mean flow velocity of the molecular gas. Figure 1 shows a schematic diagram of the system modelled in this work.

In the low-density regime, the time evolution of the one-particle velocity distribution function $f(\mathbf{r}, \mathbf{v}, t)$ of the granular gas is given by the Boltzmann kinetic equation. Since the granular particles collide among themselves and with the particles of the molecular gas, in the absence of external forces the velocity distribution f verifies the kinetic equation

$$\frac{\partial f}{\partial t} + \mathbf{v} \cdot \nabla f = J[f, f] + J_g[f, f_g]. \quad (2.2)$$

Here, the Boltzmann collision operator $J[f, f]$ gives the rate of change of the distribution f due to binary *inelastic* collisions between granular particles. On the other hand, the Boltzmann-Lorentz operator $J_g[f, f_g]$ accounts for the rate of change of the distribution f due to *elastic* collisions between granular and molecular gas particles.

The explicit form of the nonlinear Boltzmann collision operator $J[f, f]$ is (Garzó 2019)

$$J[\mathbf{v}_1|f, f] = \sigma^{d-1} \int d\mathbf{v}_2 \int d\hat{\boldsymbol{\sigma}} \Theta(\hat{\boldsymbol{\sigma}} \cdot \mathbf{g}_{12})(\hat{\boldsymbol{\sigma}} \cdot \mathbf{g}_{12}) [\alpha^{-2} f(\mathbf{v}_1'') f(\mathbf{v}_2'') - f(\mathbf{v}_1) f(\mathbf{v}_2)], \quad (2.3)$$

where $\mathbf{g}_{12} = \mathbf{v}_1 - \mathbf{v}_2$ is the relative velocity, $\hat{\boldsymbol{\sigma}}$ is a unit vector along the line of centers of the two spheres at contact, and Θ is the Heaviside step function. In Eq. (2.3), the double primes denote pre-collisional velocities. The relationship between pre-collisional $(\mathbf{v}_1'', \mathbf{v}_2'')$

and post-collisional $(\mathbf{v}_1, \mathbf{v}_2)$ velocities is

$$\mathbf{v}_1'' = \mathbf{v}_1 - \frac{1+\alpha}{2\alpha}(\hat{\boldsymbol{\sigma}} \cdot \mathbf{g}_{12})\hat{\boldsymbol{\sigma}}, \quad \mathbf{v}_2'' = \mathbf{v}_2 + \frac{1+\alpha}{2\alpha}(\hat{\boldsymbol{\sigma}} \cdot \mathbf{g}_{12})\hat{\boldsymbol{\sigma}}. \quad (2.4)$$

The form of the linear Boltzmann-Lorentz collision operator $J_g[f, f_g]$ is (Garzó 2019; Résibois & de Leener 1977)

$$J_g[\mathbf{v}_1|f, f_g] = \bar{\sigma}^{d-1} \int d\mathbf{v}_2 \int d\hat{\boldsymbol{\sigma}} \Theta(\hat{\boldsymbol{\sigma}} \cdot \mathbf{g}_{12})(\hat{\boldsymbol{\sigma}} \cdot \mathbf{g}_{12}) [f(\mathbf{v}_1'')f_g(\mathbf{v}_2'') - f(\mathbf{v}_1)f_g(\mathbf{v}_2)], \quad (2.5)$$

where $\bar{\sigma} = (\sigma + \sigma_g)/2$. In Eq. (2.5), the relationship between $(\mathbf{v}_1'', \mathbf{v}_2'')$ and $(\mathbf{v}_1, \mathbf{v}_2)$ is

$$\mathbf{v}_1'' = \mathbf{v}_1 - 2\mu_g(\hat{\boldsymbol{\sigma}} \cdot \mathbf{g}_{12})\hat{\boldsymbol{\sigma}}, \quad \mathbf{v}_2'' = \mathbf{v}_2 + 2\mu(\hat{\boldsymbol{\sigma}} \cdot \mathbf{g}_{12})\hat{\boldsymbol{\sigma}}, \quad (2.6)$$

where $\mu_g = m_g/(m + m_g)$ and $\mu = m/(m + m_g)$.

The relevant hydrodynamic fields of the granular gas are the number density $n(\mathbf{r}; t)$, the mean flow velocity $\mathbf{U}(\mathbf{r}; t)$, and the granular temperature $T(\mathbf{r}; t)$. They are defined, respectively, as

$$\{n, n\mathbf{U}, nT\} = \int d\mathbf{v} \{1, \mathbf{v}, mV^2\} f(\mathbf{v}), \quad (2.7)$$

where $\mathbf{V} = \mathbf{v} - \mathbf{U}$ is the peculiar velocity. In general, the mean flow velocity \mathbf{U} of solid particles is different from the mean flow velocity \mathbf{U}_g of molecular gas particles. As we will show later, the difference $\mathbf{U} - \mathbf{U}_g$ induces a nonvanishing contribution to the heat flux.

The macroscopic balance equations for the granular gas are obtained by multiplying Eq. (2.2) by $\{1, \mathbf{v}, mV^2\}$ and integrating over velocity. The result is

$$D_t n + n \nabla \cdot \mathbf{U} = 0, \quad (2.8)$$

$$\rho D_t \mathbf{U} = -\nabla \cdot \mathbf{P} + \mathcal{F}[f], \quad (2.9)$$

$$D_t T + \frac{2}{dn} (\nabla \cdot \mathbf{q} + \mathbf{P} : \nabla \mathbf{U}) = -T\zeta - T\zeta_g. \quad (2.10)$$

Here, $D_t = \partial_t + \mathbf{U} \cdot \nabla$ is the material derivative, $\rho = mn$ is the mass density of solid particles, and the pressure tensor \mathbf{P} and the heat flux vector \mathbf{q} are given, respectively, as

$$\mathbf{P} = \int d\mathbf{v} m \mathbf{V} \mathbf{V} f(\mathbf{v}), \quad (2.11)$$

$$\mathbf{q} = \int d\mathbf{v} \frac{m}{2} V^2 \mathbf{V} f(\mathbf{v}). \quad (2.12)$$

Since the Boltzmann-Lorentz collision term $J_g[f, f_g]$ does not conserve momentum, then the production of momentum $\mathcal{F}[f]$ is in general different from zero. It is defined as

$$\mathcal{F}[f] = \int d\mathbf{v} m \mathbf{V} J_g[f, f_g] = -\frac{2\pi^{(d-1)/2}}{\Gamma\left(\frac{d+3}{2}\right)} m_g \mu \bar{\sigma}^{d-1} \int d\mathbf{V}_1 \int d\mathbf{V}_2 g_{12} \mathbf{g}_{12} f(\mathbf{V}_1) f_g(\mathbf{V}_2). \quad (2.13)$$

In addition, the partial production rates ζ and ζ_g are given, respectively, as

$$\zeta = -\frac{m}{dnT} \int d\mathbf{v} V^2 J[\mathbf{v}|f, f], \quad (2.14)$$

$$\zeta_g = -\frac{m}{dnT} \int d\mathbf{v} V^2 J_g[\mathbf{v}|f, f_g]. \quad (2.15)$$

The cooling rate ζ gives the rate of kinetic energy loss due to inelastic collisions between particles of the granular gas. It vanishes for inelastic collisions. The term ζ_g gives the transfer of kinetic energy between the particles of the granular and molecular gas. It vanishes when the granular and molecular gas are at the same temperature ($T_g = T$).

2.1. Brownian limit ($m/m_g \rightarrow \infty$)

The suspension model defined by the Boltzmann equation (2.2) applies in principle for arbitrary values of the mass ratio m/m_g . On the other hand, a physically interesting situation arises in the so-called Brownian limit, namely, when the granular particles are much heavier than the particles of the surrounding molecular gas ($m/m_g \rightarrow \infty$). In this case, a Kramers–Moyal expansion (Résibois & de Leener 1977; Rodríguez *et al.* 1983; McLennan 1989) in the velocity jumps $\delta \mathbf{v} = (2/(1 + m/m_g))(\hat{\boldsymbol{\sigma}} \cdot \mathbf{g}_{12})\mathbf{g}_{12}$ allows us to approximate the Boltzmann–Lorentz operator $J_g[\mathbf{v}|f, f_g]$ by the Fokker–Planck operator $J_g^{\text{FP}}[\mathbf{v}|f, f_g]$ (Résibois & de Leener 1977; Rodríguez *et al.* 1983; McLennan 1989; Brey *et al.* 1999; Sarracino *et al.* 2010):

$$J_g[f, f_g] \rightarrow J_g^{\text{FP}}[f, f_g] = \gamma \frac{\partial}{\partial \mathbf{v}} \cdot \left(\mathbf{v} + \frac{T_g}{m} \frac{\partial}{\partial \mathbf{v}} \right) f(\mathbf{v}), \quad (2.16)$$

where the friction coefficient γ is defined as

$$\gamma = \frac{4\pi^{(d-1)/2}}{d\Gamma\left(\frac{d}{2}\right)} \left(\frac{m_g}{m}\right)^{1/2} \left(\frac{2T_g}{m}\right)^{1/2} n_g \bar{\sigma}^{d-1}. \quad (2.17)$$

Upon obtaining Eqs. (2.16)–(2.17), it has been assumed that $\mathbf{U}_g = \mathbf{0}$ and a Maxwellian distribution for the distribution $f(\mathbf{v})$ of the granular gas.

Most of the suspension models employed in the granular literature to fully account for the influence of the interstitial molecular fluid on the dynamics of grains are based on the replacement of $J_g[f, f_g]$ by the Fokker–Planck operator (2.16) (Koch & Hill 2001). More specifically, for general inhomogeneous states, the impact of the background molecular gas on solid particles is through an effective force composed by three different terms: (i) a term proportional to the difference $\Delta \mathbf{U} = \mathbf{U} - \mathbf{U}_g$, (ii) a drag force term mimicking the friction of grains on the viscous interstitial gas, and (iii) a stochastic Langevin-like term accounting for the energy gained by grains due to their interactions with particles of the molecular gas (neighbouring particles effect) (Garzó *et al.* 2012). This yields the following kinetic equation for gas-solid suspensions †

$$\frac{\partial f}{\partial t} + \mathbf{v} \cdot \nabla f - \gamma \Delta \mathbf{U} \cdot \frac{\partial f}{\partial \mathbf{v}} - \gamma \frac{\partial}{\partial \mathbf{v}} \cdot \mathbf{V} f - \gamma \frac{T_g}{m} \frac{\partial^2 f}{\partial v^2} = J[\mathbf{v}|f, f]. \quad (2.18)$$

The Boltzmann equation (2.18) has been solved by means of the Chapman–Enskog method (Chapman & Cowling 1970) to first-order in spatial gradients. Explicit forms for the Navier–Stokes–Fourier transport coefficients have been obtained in steady-state conditions, namely, when the cooling terms are compensated for by the energy gained by the solid particles due to their collisions with the bath particles (Garzó *et al.* 2013; Gómez González & Garzó 2019). Thus, the results derived in the present paper must be

† There are three different scalars (β, γ, ξ) in the suspension model proposed by Garzó *et al.* (2012); each one of the coefficients is associated with the different terms of the fluid-solid force. For the sake of simplicity, the results derived by Gómez González & Garzó (2019) were obtained by assuming that $\beta = \gamma = \xi$.

consistent with those previously obtained by Gómez González & Garzó (2019) when the limit $m_g/m \rightarrow 0$ is considered in our general results.

3. Homogeneous steady state

As a first step and before studying inhomogeneous states, we consider the HSS. The HSS is the reference base state (zeroth-order approximation) used in the Chapman–Enskog perturbation method (Chapman & Cowling 1970). Therefore, its investigation is of great importance. The HSS was widely analysed by Santos (2003) for a three-dimensional granular gas. Here, we extend these calculations to a general dimension d .

In the HSS, the density n and temperature T are spatially uniform, and with an appropriate selection of the frame reference, the mean flow velocities vanish ($\mathbf{U} = \mathbf{U}_g = \mathbf{0}$). Consequently, the Boltzmann equation (2.2) reads

$$\frac{\partial f}{\partial t} = J[f, f] + J_g[f, f_g]. \quad (3.1)$$

Moreover, the velocity distribution $f(\mathbf{v})$ of the granular gas is isotropic in \mathbf{v} so that the production of momentum $\mathcal{F}[f] = \mathbf{0}$, according to Eq. (2.13). Thus, the only nontrivial balance equation is that of the temperature (2.10):

$$\frac{\partial \ln T}{\partial t} = -(\zeta + \zeta_g). \quad (3.2)$$

As mentioned in section 2, since collisions between granular particles are inelastic, then the cooling rate $\zeta > 0$. Collisions between particles of granular and molecular gases are elastic and so, the total kinetic energy of two colliding particles is conserved. On the other hand, since in the steady state the background gas acts as a thermostat, then the mean kinetic energy of granular particles is smaller than that of the molecular gas and so, $T < T_g$. This necessarily implies that $\zeta_g < 0$. Therefore, in the *steady* state, the terms ζ and ζ_g exactly compensates each other and one gets the steady-state condition

$$\zeta + \zeta_g = 0. \quad (3.3)$$

The condition (3.3) allows one to get the steady granular temperature T . However, according to the definitions (2.14) and (2.15), the determination of ζ and ζ_g requires to know the velocity distribution $f(\mathbf{v})$. For inelastic collisions ($\alpha \neq 1$), to date the solution of the Boltzmann equation (3.1) has not been found. On the other hand, a good estimate of ζ and ζ_g can be obtained when the first-Sonine approximation to f is considered (Brilliantov & Pöschel 2004). In this approximation, $f(\mathbf{v})$ is given by

$$f(\mathbf{v}) \simeq f_{\text{MB}}(\mathbf{v}) \left\{ 1 + \frac{a_2}{2} \left[\left(\frac{mv^2}{2T} \right)^2 - (d+2) \frac{mv^2}{2T} + \frac{d(d+2)}{4} \right] \right\}, \quad (3.4)$$

where

$$f_{\text{MB}}(\mathbf{v}) = n \left(\frac{m}{2\pi T} \right)^{d/2} \exp \left(- \frac{mv^2}{2T} \right) \quad (3.5)$$

is the Maxwell–Boltzmann distribution and

$$a_2 = \frac{1}{d(d+2)} \frac{m^2}{nT^2} \int d\mathbf{v} v^4 f(\mathbf{v}) - 1 \quad (3.6)$$

is the kurtosis or fourth cumulant. This quantity measures the departure of the distribution $f(\mathbf{v})$ from its Maxwellian form $f_{\text{MB}}(\mathbf{v})$. From experience with the dry granular case (van Noije & Ernst 1998; Garzó & Dufty 1999; Montanero & Santos 2000; Santos

& Montanero 2009), the magnitude of the cumulant a_2 is expected to be very small and so, the Sonine approximation (3.4) to the distribution f turns out to be reliable. In the case that $|a_2|$ does not remain small for high inelasticity, one should include cumulants of higher order in the Sonine polynomial expansion of f . However, the possible lack of convergence of the Sonine polynomial expansion for very small values of the coefficient of restitution (Brilliantov & Pöschel 2006*a,b*) puts on doubt the reliability of the Sonine expansion in the high inelasticity region. Here, we will restrict to values of α where $|a_2|$ remains relatively small.

The expressions of ζ and ζ_g can be now obtained by replacing in Eqs. (2.14) and (2.15) f by its Sonine approximation (3.4). Retaining only linear terms in a_2 , the forms of the dimensionless production rates

$$\zeta^* = \frac{\ell \zeta}{v_{\text{th}}}, \quad \zeta_g^* = \frac{\ell \zeta_g}{v_{\text{th}}} \quad (3.7)$$

can be written as (van Noije & Ernst 1998; Brilliantov & Pöschel 2006*a*)

$$\zeta^* = \tilde{\zeta}^{(0)} + \tilde{\zeta}^{(1)} a_2, \quad \zeta_g^* = \tilde{\zeta}_g^{(0)} + \tilde{\zeta}_g^{(1)} a_2, \quad (3.8)$$

where

$$\tilde{\zeta}^{(0)} = \frac{\sqrt{2}\pi^{(d-1)/2}}{d\Gamma\left(\frac{d}{2}\right)}(1 - \alpha^2), \quad \tilde{\zeta}^{(1)} = \frac{3}{16}\tilde{\zeta}^{(0)}, \quad (3.9)$$

$$\tilde{\zeta}_g^{(0)} = 2x(1 - x^2)\left(\frac{\mu T}{T_g}\right)^{1/2} \gamma^*, \quad \tilde{\zeta}_g^{(1)} = \frac{\mu_g}{8}x^{-3}\left[x^2(4 - 3\mu_g) - \mu_g\right]\left(\frac{\mu T}{T_g}\right)^{1/2} \gamma^*. \quad (3.10)$$

Here, $\ell = 1/(n\sigma^{d-1})$ is proportional to the mean free path of hard spheres, $v_{\text{th}} = \sqrt{2T/m}$ is the thermal velocity, and we have introduced the auxiliary parameters

$$x = \left(\mu_g + \mu \frac{T_g}{T}\right)^{1/2}, \quad (3.11)$$

and

$$\gamma^* = \varepsilon \left(\frac{T_g}{T}\right)^{1/2}, \quad \varepsilon = \frac{\ell \gamma}{\sqrt{2T_g/m}} = \frac{\sqrt{2}\pi^{d/2}}{2^d d \Gamma\left(\frac{d}{2}\right)} \frac{1}{\phi \sqrt{T_g^*}}. \quad (3.12)$$

Here,

$$\phi = \frac{\pi^{d/2}}{2^{d-1} d \Gamma\left(\frac{d}{2}\right)} n \sigma^d \quad (3.13)$$

is the solid volume fraction and

$$T_g^* = \frac{T_g}{m \sigma^2 \gamma^2} \quad (3.14)$$

is the (reduced) bath temperature. The (reduced) friction coefficient γ^* characterises the rate at which the collisions between grains and molecular particles occur. Equations (3.9) and (3.10) agree with those obtained by Santos (2003) for $d = 3$.

To close the problem, we have to determine the kurtosis a_2 . In this case, one has to compute the collisional moments

$$A \equiv \int d\mathbf{v} v^4 J[f, f], \quad A_g \equiv \int d\mathbf{v} v^4 J_g[f, f_g]. \quad (3.15)$$

In the steady state, apart from Eq. (3.3), one has the additional condition

$$\Lambda + \Lambda_g = 0. \quad (3.16)$$

The moments Λ and Λ_g have been obtained in previous works (van Noije & Ernst 1998; Brilliantov & Pöschel 2006a; Garzó *et al.* 2009; Garzó 2019) by replacing f by its first Sonine form (3.4) and neglecting nonlinear terms in a_2 . In terms of the (reduced) friction coefficient γ^* , the expressions of

$$\{\Lambda^*, \Lambda_g^*\} = \frac{\ell}{nv_{\text{th}}^5} \{\Lambda, \Lambda_g\} \quad (3.17)$$

are given by

$$\Lambda^* = \Lambda^{(0)} + \Lambda^{(1)} a_2, \quad \Lambda_g^* = \Lambda_g^{(0)} + \Lambda_g^{(1)} a_2, \quad (3.18)$$

where

$$\Lambda^{(0)} = -\frac{\pi^{(d-1)/2}}{\sqrt{2}\Gamma\left(\frac{d}{2}\right)} \left(d + \frac{3}{2} + \alpha^2\right) (1 - \alpha^2), \quad (3.19)$$

$$\Lambda^{(1)} = -\frac{\pi^{(d-1)/2}}{\sqrt{2}\Gamma\left(\frac{d}{2}\right)} \left[\frac{3}{32} (10d + 39 + 10\alpha^2) + \frac{d-1}{1-\alpha}\right] (1 - \alpha^2), \quad (3.20)$$

$$\Lambda_g^{(0)} = dx^{-1} (x^2 - 1) [8\mu_g x^4 + x^2 (d + 2 - 8\mu_g) + \mu_g] \left(\frac{\mu T}{T_g}\right)^{1/2} \gamma^*, \quad (3.21)$$

$$\begin{aligned} \Lambda_g^{(1)} = \frac{d}{8} x^{-5} & \left\{ 4x^6 [30\mu_g^3 - 48\mu_g^2 + 3(d+8)\mu_g - 2(d+2)] + \mu_g x^4 [-48\mu_g^2 \right. \\ & \left. + 3(d+26)\mu_g - 8(d+5)] + \mu_g^2 x^2 (d+14-9\mu_g) - 3\mu_g^3 \right\} \left(\frac{\mu T}{T_g}\right)^{1/2} \gamma^*. \end{aligned} \quad (3.22)$$

For hard spheres ($d = 3$), Eqs. (3.19)–(3.22) are consistent with those previously obtained by Santos (2003).

Inserting Eqs. (3.8)–(3.10) and (3.18)–(3.22) into Eqs. (3.3) and (3.16), respectively, one gets the set of coupled equations:

$$\tilde{\zeta}^{(0)} + \tilde{\zeta}_g^{(0)} + \left(\tilde{\zeta}^{(1)} + \tilde{\zeta}_g^{(1)}\right) a_2 = 0, \quad (3.23)$$

$$\Lambda^{(0)} + \Lambda_g^{(0)} + \left(\Lambda^{(1)} + \Lambda_g^{(1)}\right) a_2 = 0. \quad (3.24)$$

Eliminating a_2 in Eqs. (3.23) and (3.24), one achieves the following closed equation for the temperature ratio T/T_g :

$$\left(\tilde{\zeta}^{(1)} + \tilde{\zeta}_g^{(1)}\right) \left(\Lambda^{(0)} + \Lambda_g^{(0)}\right) = \left(\tilde{\zeta}^{(0)} + \tilde{\zeta}_g^{(0)}\right) \left(\Lambda^{(1)} + \Lambda_g^{(1)}\right). \quad (3.25)$$

For given values of α , ϕ , and T_g^* , the numerical solution of Eq. (3.25) gives T/T_g . Once the temperature ratio is determined, the cumulant a_2 is simply given by

$$a_2 = -\frac{\tilde{\zeta}^{(0)} + \tilde{\zeta}_g^{(0)}}{\tilde{\zeta}^{(1)} + \tilde{\zeta}_g^{(1)}} = -\frac{\Lambda^{(0)} + \Lambda_g^{(0)}}{\Lambda^{(1)} + \Lambda_g^{(1)}}. \quad (3.26)$$

3.1. Brownian limit

Before illustrating the dependence of T/T_g and a_2 on α for given values of ϕ and T_g^* , it is interesting to consider the Brownian limit $m_g/m \rightarrow 0$. In this limiting case, $\mu_g \rightarrow 0$, $\mu \rightarrow 1$, $x \rightarrow \sqrt{T_g/T}$, and so

$$\tilde{\zeta}_g^{(0)} \rightarrow 2 \left(1 - \frac{T_g}{T}\right) \gamma^*, \quad \tilde{\zeta}_g^{(1)} \rightarrow 0, \quad (3.27)$$

$$\Lambda_g^{(0)} \rightarrow d(d+2) \left(\frac{T_g}{T} - 1\right) \gamma^*, \quad \Lambda_g^{(1)} \rightarrow -d(d+2) \gamma^*. \quad (3.28)$$

Taking into these results, the set of equations (3.23) and (3.24) can be written in the Brownian limit as

$$2\gamma^* \left(\frac{T_g}{T} - 1\right) = \zeta^*, \quad d(d+2) \left(\gamma^* a_2 - \frac{1}{2} \zeta^*\right) = \Lambda^*. \quad (3.29)$$

These equations are the same as those derived by Gómez González & Garzó (2019) [see Eqs. (29) and (34) of this paper] by using the suspension model (2.18). This shows the consistency of the present results in the HSS with those obtained in the Brownian limit.

3.2. DSMC simulations

The previous analytical results have been obtained by using the first-Sonine approximation (3.4) to f . Thus, it is worth solving the Boltzmann kinetic equation by means of an alternative method to test the reliability of the theoretical predictions for T/T_g [Eq. (3.25)] and a_2 [Eq. (3.26)]. The Direct Simulation Monte Carlo (DSMC) method developed by Bird (1994) is considered here to numerically solve the Boltzmann equation in the homogeneous state. As described in section 1, we treat in this paper the molecular gas as a thermostat in the sense that its state is not perturbed by the presence of grains. Therefore, the collision stage in the DSMC method must be slightly modified to accurately reproduce Eq. (3.1). We follow similar steps as proposed by Montanero & Garzó (2002) to numerically solve the Boltzmann–Enskog equation of a homogeneous granular mixture.

The simulation is initiated by drawing the particle velocities from a Maxwellian distribution at temperature T_g following the Box–Muller transform (Box & Muller 1958). Since the granular gas is assumed to be spatially homogeneous, only the collision stage is described here. The procedure can be summarised as follows:

(i) A required number of $N_j^{\delta t}$ candidate pairs to collide in a time δt is selected. This number is given by[†] (Montanero & Garzó 2002)

$$N_j^{\delta t} = j \frac{2^{d-3} d \Gamma\left(\frac{d}{2}\right) (\sigma + \sigma_j)^2}{\pi^{d/2} \sigma^d} N_j \phi g_j^{\max} \delta t, \quad (3.30)$$

where $j = 1$ ($j = 2$) refers to a granular (molecular) particle. Namely, $N_1^{\delta t}$ refers to granular-granular collisions, while $N_2^{\delta t}$ refers to granular-molecular collisions. Here, N_j is the total number of particles of species j and g_j^{\max} is an upper bound of the average relative velocity. A good estimate is $g_j^{\max} = C v_j^{\text{th}}$, where $v_j^{\text{th}} = \sqrt{2T_g/\bar{m}}$ is the mean thermal velocity, $\bar{m} = (m + m_j)/2$, and C is a constant, e.g., $C = 5$ (Bird 1994). Note that in Eq. (3.30) collisions among molecular particles themselves have been neglected.

[†] In contrast to the work of Montanero & Garzó (2002), we consider here a very dilute system and so, the pair correlation functions are set equal to 1.

- (ii) A colliding direction $\hat{\sigma}_j$ is randomly selected with equiprobability.
- (iii) The collision is accepted if

$$|\hat{\sigma}_j \cdot \mathbf{g}_{12}| = |\hat{\sigma}_j \cdot (\mathbf{v}_1 - \mathbf{v}_2)| > U(0, 1)g_j^{\max}, \quad (3.31)$$

where $U(0, 1)$ is a random number uniformly distributed in $[0, 1]$.

- (iv) If the collision is accepted, only granular particles velocities are updated according to the relationships (2.4) for $j = 1$ and (2.6) for $j = 2$.

The former procedure constitutes an intermediate method between Bird's (Bird 1994) and Nanbu's (Nanbu 1986) schemes since in the latter only one of the colliding particles changes its velocity. However, as pointed out by Montanero & Santos (1997), both schemes are equivalent and equally useful to solve the Boltzmann equation since in both techniques momentum is conserved on average. Thus, we do not need to account for collisions among molecular particles themselves because $n/n_g \ll 1$ and the computational cost would be very expensive.

Moreover, in the theory all the mechanical information of the molecular gas (with the exception the mass ratio m/m_g) is enclosed in the (reduced) friction coefficient γ^* throughout the reduced (bath) temperature T_g^* . Let us denote by N_g and N the total number of granular and molecular particles, respectively. Since $N/N_g = n/n_g$, then σ and σ_g are related by

$$\sigma_g = \left[\left(\frac{\sqrt{\pi}}{4\sqrt{2}} \frac{N}{N_g} \sqrt{\frac{m}{m_g}} \frac{1}{\phi \sqrt{T_g^*}} \right)^{1/(d-1)} - 1 \right] \sigma. \quad (3.32)$$

Upon deriving Eq. (3.32) use has been made of the relationships

$$n = \frac{2^{d-1} d \Gamma(\frac{d}{2})}{\pi^{d/2}} \sigma^{-d} \phi, \quad n_g = \frac{d \Gamma(\frac{d}{2})}{4\pi^{(d-1)/2}} \left(\frac{m}{m_g} \right)^{1/2} \left(\frac{m}{2T_g} \right)^{1/2} \sigma^{1-d} \gamma. \quad (3.33)$$

Equation (3.32) establishes a constraint in the inputs regarding the molecular gas. For this reason, once the inputs appearing in the theory ($d, m/m_g, T_g^*, \phi$) are fixed, then we choose N_g in such a way that $N_g/N \gg 1$ and $\sigma_g/\sigma > 0$.

Figure 2 shows the dependence of the temperature ratio $\chi \equiv T/T_g$ on the coefficient of restitution α for several values of the mass ratio m/m_g . A very dilute ensemble ($\phi = 0.001$) of hard spheres ($d = 3$) is considered. The value of the reduced (bath) temperature T_g^* is selected so that collisions between grains and with the interstitial gas are both relevant on the dynamics of grains. Here, we chose $T_g^* = 1000$. The lines are the theoretical results obtained by numerically solving Eq. (3.25). The symbols refer to DSMC simulations performed following the method described above. Four different values of the mass ratio m/m_g are considered ($m/m_g = 1, 5, 10$, and 50). For the sake of comparison, the dotted line shows the α -dependence of χ achieved in the Brownian limit, namely when considering the Langevin-like suspension model described in Eq. (2.18) (Gómez González & Garzó 2019). In addition, black circles refer to DSMC simulations performed by employing the model (2.18). To carry on these kind of simulations, the influence of the external fluid on grains is taken into account by updating the velocity of every single grain each time step δt according to (Khalil & Garzó 2014; Gómez González *et al.* 2021):

$$\mathbf{v} \rightarrow e^{-\gamma \delta t} \mathbf{v} + \left(\frac{6\gamma T_g \delta t}{m} \right)^{1/2} \mathbf{U}[-1, 1]. \quad (3.34)$$

Here, \mathbf{U} is an uniformly distributed random vector in $[-1, 1]^3$. Equation (3.34) converges

to the Fokker–Plank operator (2.16) when a time step δt much smaller than the mean free time between collisions is considered (Khalil & Garzó 2014).

Figure 2 ensures the reliability of the results derived in this section for two different reasons: (i) a good agreement between theory and simulation is found and (ii) the convergence towards the Brownian limit can be clearly observed. Surprisingly, this convergence is fully reached for relatively small values of the mass ratio ($m/m_g \approx 50$) in contrast to the results reported by Santos (2003). Another unexpected result concerns the lack of energy equipartition ($T \neq T_g$) (Barrat & Trizac 2002; Dahl *et al.* 2002). One expects the temperature of the granular and molecular gases to be similar when the particles that composed them are mechanically comparable. However, according to Eq. (2.6), the transmission of energy per individual collision from a molecular particle to a grain is bigger when their masses are similar. Nonetheless, the constraint imposed by Eq. (3.32) leads to a dependence of N/N_g on the mass ratio m/m_g for fixed σ_g . Thus, $N_g/N \propto m/m_g$ and so, the number density of the molecular gas increases as increasing the mass ratio. This way, the mean force exerted by the molecular particles on the grains is greater and therefore, the thermalisation caused by the presence of the interstitial fluid is much more effective. The steady temperature ratio χ is reached when the energy lost by collisions is compensated for by the energy provided by the bath. Hence, the nonequipartition of energy turns out then to be remarkable to small values of m/m_g and α . The former contrasts again with the results plotted in Fig. 2. of Santos (2003). However, as discussed in this section, for hard spheres ($d = 3$) the results obtained in the HSS are consistent with those reported by Santos (2003). Consequently, the discrepancies found both in the convergence to the Brownian limit and in the dependence of the energy nonequipartition on the mass ratio are just a matter of the way of scaling the variables. In our study, we have introduced γ^* in Eq. (3.23) as an auxiliary dimensionless variable for the sake of comparison with the results obtained by Gómez González & Garzó (2019).

Figure 3 illustrates the α -dependence of the cumulant a_2 for the same parameters as in Fig. 2. As can be seen, the breakdown of energy equipartition makes the system to be in an out-of-equilibrium state where $f \neq f_{\text{MB}}$. On the other hand, we find that the magnitude of a_2 is in general small for not quite large inelasticity (for instance, $\alpha \gtrsim 0.5$); this result supports the assumption of a low-order truncation (first Sonine approximation) in the polynomial expansion of the distribution function. In addition, the departure of f from its Maxwellian form accentuates when decreasing the mass ratio m/m_g in the same way as the steady granular temperature T moves away from its equilibrium value T_g reached for elastic collisions ($\alpha = 1$). Thus, the magnitude of a_2 increases as m/m_g decreases and so, higher-order coefficients in the Sonine approximation could turn out to be significant for strong inelasticity. This could be the reason why we observe some discrepancies between theory and DSMC simulations in Figs. 2 and 3 for $m/m_g = 1$, specially in the case of a_2 . However, these discrepancies are of the same order than those found for dry granular gases (Montanero & Garzó 2002).

4. Chapman–Enskog expansion. First-order approximation

We perturb now the homogeneous state by small spatial gradients. These perturbations will give nonzero contributions to the pressure tensor and the heat flux vector. The determination of these fluxes will allow us to identify the Navier–Stokes–Fourier transport coefficients of the granular gas. For times longer than the mean free time, we assume that the system evolves towards a *hydrodynamic* regime where the distribution function $f(\mathbf{r}, \mathbf{v}; t)$ adopts the form of a *normal* or hydrodynamic solution. This means that all space and time dependence of f only occurs through the hydrodynamic fields n , \mathbf{U} , and

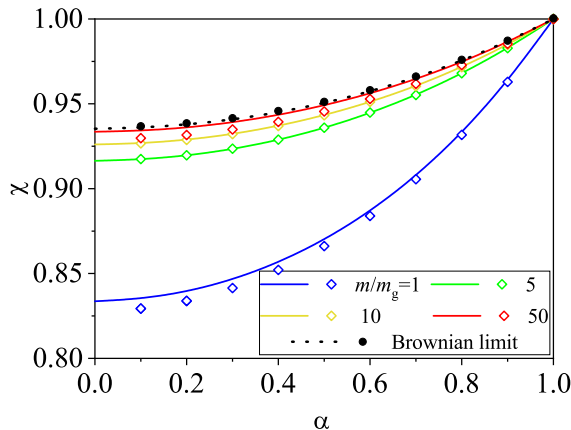


FIGURE 2. Temperature ratio $\chi \equiv T/T_g$ versus the coefficient of normal restitution α for $d = 3$, $\phi = 0.001$, $T_g^* = 1000$, and four different values of the mass ratio m/m_g [from top to bottom, $m/m_g = 50, 10, 5$, and 1]. The solid lines are the theoretical results obtained by numerically solving Eq. (3.25) and the symbols are the Monte Carlo simulation results. The dotted line is the result obtained by Gómez González & Garzó (2019) by using the Langevin-like suspension model (2.18) while black circles refer to DSMC simulations implemented using the time-driven approach (3.34).

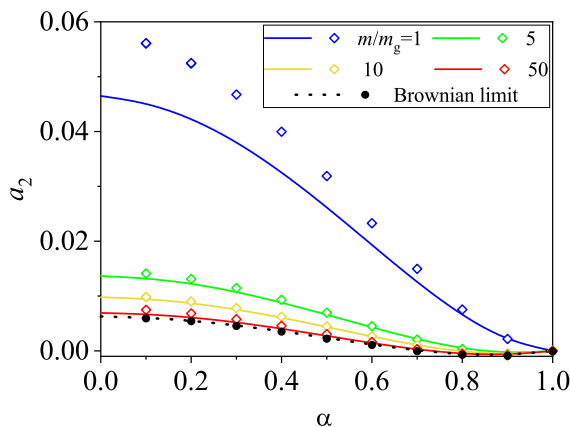


FIGURE 3. Plot of the fourth cumulant a_2 as a function of the coefficient of normal restitution α for $d = 3$, $\phi = 0.001$, $T_g^* = 1000$, and four different values of the mass ratio m/m_g [from top to bottom, $m/m_g = 1, 5, 10$, and 50]. The solid lines are the theoretical results obtained from Eq. (3.25) and the symbols are the Monte Carlo simulation results. The dotted line is the result obtained by Gómez González & Garzó (2019) by using the Langevin-like suspension model (2.18) while black circles refer to DSMC simulations implemented using the time-driven approach (3.34).

T :

$$f(\mathbf{r}, \mathbf{v}, t) = f[\mathbf{v}|n(t), \mathbf{U}(t), T(t)]. \quad (4.1)$$

The notation on the right hand side indicates a functional dependence on the density, flow velocity and temperature. For low Knudsen numbers (i.e., small spatial variations), the functional dependence (4.1) can be made local in space by means of an expansion in powers of the gradients ∇n , $\nabla \mathbf{U}$, and ∇T . In this case, f can be expressed in the form

$$f = f^{(0)} + f^{(1)} + f^{(2)} + \dots, \quad (4.2)$$

where the approximation $f^{(k)}$ is of order k in spatial gradients. Here, since we are interested in the Navier–Stokes hydrodynamic equations, only terms up to first order in gradients will be considered in the constitutive equations for the momentum and heat fluxes.

On the other hand, inasmuch as after a transient period and in the absence of spatial gradients, the mean flow velocity \mathbf{U} of the granular gas tends to the mean flow velocity \mathbf{U}_g of the molecular gas, then the velocity difference term $\Delta\mathbf{U}$ must be considered to be at least of first order in the spatial gradients. This implies that the Maxwellian distribution $f_g(\mathbf{v})$ must be also expanded as

$$f_g(\mathbf{v}) = f_g^{(0)}(\mathbf{V}) + f_g^{(1)}(\mathbf{V}) + \dots, \quad (4.3)$$

where

$$f_g^{(0)}(\mathbf{V}) = n_g \left(\frac{m_g}{2\pi T_g} \right)^{d/2} \exp \left(- \frac{m_g V^2}{2T_g} \right), \quad (4.4)$$

and

$$f_g^{(1)}(\mathbf{V}) = - \frac{m_g}{T_g} \mathbf{V} \cdot \Delta\mathbf{U} f_g^{(0)}(\mathbf{V}). \quad (4.5)$$

According to the expansion (4.1), the pressure tensor P_{ij} , the heat flux \mathbf{q} , and the partial production rates ζ and ζ_g must be also expressed accordingly to the perturbation scheme in the forms

$$P_{ij} = P_{ij}^{(0)} + P_{ij}^{(1)} + \dots, \quad \mathbf{q} = \mathbf{q}^{(0)} + \mathbf{q}^{(1)} + \dots, \quad \zeta = \zeta^{(0)} + \zeta^{(1)} + \dots, \quad \zeta_g = \zeta_g^{(0)} + \zeta_g^{(1)} + \dots \quad (4.6)$$

In addition, the time derivative ∂_t is also given as

$$\partial_t = \partial_t^{(0)} + \partial_t^{(1)} + \dots, \quad (4.7)$$

where the action of the operators $\partial_t^{(k)}$ on the hydrodynamic fields can be identified when the expansions (4.6) of the fluxes and the production rates are considered in the macroscopic balance equations (2.8)–(2.10). This is the conventional Chapman–Enskog method (Chapman & Cowling 1970; Garzó 2019) for solving the Boltzmann kinetic equation.

As usual in the Chapman–Enskog method (Chapman & Cowling 1970), the zeroth-order distribution function $f^{(0)}$ defines the hydrodynamic fields n , \mathbf{U} , and T :

$$\{n, n\mathbf{U}, dnT\} = \int d\mathbf{v} \left\{ 1, \mathbf{v}, \frac{m}{2} V^2 \right\} f^{(0)}(\mathbf{V}). \quad (4.8)$$

The requirements (4.8) must be fulfilled at any order in the expansion and so, the distributions $f^{(k)}$ ($k \geq 1$) must thus obey the orthogonality conditions

$$\int d\mathbf{v} \left\{ 1, \mathbf{v}, \frac{m}{2} V^2 \right\} f^{(k)}(\mathbf{V}) = \{0, \mathbf{0}, 0\}. \quad (4.9)$$

These are the usual solubility conditions of the Chapman–Enskog scheme.

4.1. Zeroth-order approximation

To zeroth-order in the expansion, the distribution $f^{(0)}$ verifies the kinetic equation

$$\partial_t^{(0)} f^{(0)} = J[f^{(0)}, f^{(0)}] + J_g[f^{(0)}, f_g^{(0)}]. \quad (4.10)$$

The conservation laws at this order give

$$\partial_t^{(0)} n = 0, \quad \partial_t^{(0)} \mathbf{U} = \mathbf{0}, \quad \partial_t^{(0)} T = -T \left(\zeta^{(0)} + \zeta_g^{(0)} \right), \quad (4.11)$$

where $\zeta^{(0)}$ and $\zeta_g^{(0)}$ are determined from Eqs. (2.14) and (2.15), respectively, with the replacements $f \rightarrow f^{(0)}$ and $f_g \rightarrow f_g^{(0)}$. In particular, as discussed in Sec. 3, an accurate approximation to both production rates is given by Eq. (3.8). In addition, upon obtaining the second relation in Eq. (4.11), we have accounted for that the distributions $f^{(0)}$ and $f_g^{(0)}$ are isotropic in \mathbf{V} and so, the zeroth-order contribution to the production of momentum vanishes ($\mathcal{F}^{(0)}[f^{(0)}] = \mathbf{0}$).

Since the zeroth-order distribution $f^{(0)}$ qualifies as a normal solution, then $\partial_t^{(0)} f^{(0)} = (\partial_T f^{(0)})(\partial_t^{(0)})$, and Eq. (4.10) can be rewritten as

$$-\left(\zeta^{(0)} + \zeta_g^{(0)}\right) T \frac{\partial f^{(0)}}{\partial T} = J[f^{(0)}, f^{(0)}] + J_g[f^{(0)}, f_g^{(0)}]. \quad (4.12)$$

Equation (4.12) has the same form as the Boltzmann equation (3.1) for a time-dependent homogeneous state, except that $f^{(0)}(\mathbf{r}, \mathbf{v}; t)$ is the *local* version of the above distribution. Dimensional analysis requires that $f^{(0)}$ has the scaled form

$$f^{(0)}(\mathbf{r}, \mathbf{v}; t) = n(\mathbf{r}; t) v_{\text{th}}(\mathbf{r}; t)^{-d} \varphi(\mathbf{c}, T/T_g), \quad (4.13)$$

where $\mathbf{c} = \mathbf{V}/v_{\text{th}}$, $v_{\text{th}}(\mathbf{r}; t) = \sqrt{2T(\mathbf{r}; t)/m}$ being the local thermal velocity. As expected, in contrast to the so-called homogeneous cooling state for (dry) granular gases (van Noije & Ernst 1998; Garzó 2019), the time dependence of the scaled distribution φ does not only occur through the scaled velocity \mathbf{c} but also through the temperature ratio T/T_g .

As mentioned before, since $f^{(0)}$ is isotropic in \mathbf{V} , the heat flux vanishes ($\mathbf{q}^{(0)} = \mathbf{0}$) and the pressure tensor $P_{ij}^{(0)} = p\delta_{ij}$, where $p = nT$ is the hydrostatic pressure. An estimate to $\zeta^{(0)}$ and $\zeta_g^{(0)}$ in the first-Sonine approximation is provided by Eqs. (3.8)–(3.10).

4.2. First-order approximation

The determination of the first-order approximation $f^{(1)}(\mathbf{r}, \mathbf{v}; t)$ follows similar steps as those made in previous works of granular gases (Brey *et al.* 1998; Garzó & Dufty 1999; Garzó *et al.* 2013; Gómez González & Garzó 2019). Some technical details involved in the derivation of the kinetic equation verifying $f^{(1)}$ are provided in the Appendix A for the interested reader. To first-order in spatial gradients, the distribution function is given by

$$f^{(1)}(\mathbf{V}) = \mathcal{A}(\mathbf{V}) \cdot \nabla \ln T + \mathcal{B}(\mathbf{V}) \cdot \nabla \ln n + \mathcal{C}_{ij} \frac{1}{2} \left(\partial_i U_j + \partial_j U_i - \frac{2}{d} \delta_{ij} \nabla \cdot \mathbf{U} \right) + \mathcal{D}(\mathbf{V}) \nabla \cdot \mathbf{U} + \mathcal{E} \cdot \Delta \mathbf{U}, \quad (4.14)$$

where the quantities \mathcal{A} , \mathcal{B} , \mathcal{C}_{ij} , \mathcal{D} , and \mathcal{E} are the solutions of the following set of coupled linear integral equations:

$$\begin{aligned} -\left(\zeta^{(0)} + \zeta_g^{(0)}\right) T \partial_T \mathcal{A}_i - \frac{1}{2} \left[\zeta^{(0)} + \zeta_g^{(0)} \left(1 + 2\chi \frac{\partial \ln \zeta_g^*}{\partial \chi} \right) \right] \mathcal{A}_i + \mathcal{L} \mathcal{A}_i - \rho^{-1} \frac{\partial f^{(0)}}{\partial V_j} \mathcal{K}_j[\mathcal{A}_i] \\ - J_g[\mathcal{A}_i, f_g^{(0)}] = \mathcal{A}_i, \end{aligned} \quad (4.15)$$

$$\begin{aligned} -\left(\zeta^{(0)} + \zeta_g^{(0)}\right) T \partial_T \mathcal{B}_i + \mathcal{L} \mathcal{B}_i - J_g[\mathcal{B}_i, f_g^{(0)}] - \rho^{-1} \frac{\partial f^{(0)}}{\partial V_j} \mathcal{K}_j[\mathcal{B}_i] = \mathcal{B}_i + \left[\zeta^{(0)} + \zeta_g^{(0)} \right. \\ \left. \times \left(1 - \varepsilon \frac{\partial \ln \zeta_g^*}{\partial \varepsilon} \right) \right] \mathcal{A}_i, \end{aligned} \quad (4.16)$$

$$- \left(\zeta^{(0)} + \zeta_g^{(0)} \right) T \partial_T \mathcal{C}_{ij} + \mathcal{L} \mathcal{C}_{ij} - \rho^{-1} \frac{\partial f^{(0)}}{\partial V_\ell} \mathcal{K}_\ell[\mathcal{C}_{ij}] - J_g[\mathcal{C}_{ij}, f_g^{(0)}] = C_{ij}, \quad (4.17)$$

$$- \left(\zeta^{(0)} + \zeta_g^{(0)} \right) T \partial_T \mathcal{D} + \mathcal{L} \mathcal{D} - (\zeta_U + \zeta_{Ug}) T \frac{\partial f^{(0)}}{\partial T} - \rho^{-1} \frac{\partial f^{(0)}}{\partial V_i} \mathcal{K}_i[\mathcal{D}] - J_g[\mathcal{D}, f_g^{(0)}] = D, \quad (4.18)$$

$$- \left(\zeta^{(0)} + \zeta_g^{(0)} \right) T \partial_T \mathcal{E}_i + \mathcal{L} \mathcal{E}_i - \rho^{-1} \frac{\partial f^{(0)}}{\partial V_j} \mathcal{K}_j[\mathcal{E}_i] - J_g[\mathcal{E}_i, f_g^{(0)}] = E_i - \frac{m_g}{T_g} J_g[f^{(0)}, \mathbf{V} f_g^{(0)}]. \quad (4.19)$$

In Eqs. (4.15)–(4.19), ζ_g^* is defined in Eq. (3.7) with the replacement $\zeta_g \rightarrow \zeta_g^{(0)}$,

$$\mathcal{L}X = - \left(J[f^{(0)}, X] + J[X, f^{(0)}] \right) \quad (4.20)$$

is the linearized Boltzmann collision operator, and

$$\mathcal{K}_i[X] = \int d\mathbf{v} \, m V_i J_g[X, f_g^{(0)}]. \quad (4.21)$$

In addition, the coefficients \mathbf{A} , \mathbf{B} , C_{ij} , D , and \mathbf{E} are functions of the peculiar velocity \mathbf{V} . They are given by

$$\mathbf{A}(\mathbf{V}) = -\mathbf{V} T \frac{\partial f^{(0)}}{\partial T} - \frac{p}{\rho} \frac{\partial f^{(0)}}{\partial \mathbf{V}}, \quad (4.22)$$

$$\mathbf{B}(\mathbf{V}) = -\mathbf{V} n \frac{\partial f^{(0)}}{\partial n} - \frac{p}{\rho} \frac{\partial f^{(0)}}{\partial \mathbf{V}}, \quad (4.23)$$

$$C_{ij}(\mathbf{V}) = V_i \frac{\partial f^{(0)}}{\partial V_j}, \quad (4.24)$$

$$D(\mathbf{V}) = \frac{1}{d} \frac{\partial}{\partial \mathbf{V}} \cdot (\mathbf{V} f^{(0)}) + \frac{2}{d} T \frac{\partial f^{(0)}}{\partial T} - f^{(0)} + n \frac{\partial f^{(0)}}{\partial n}, \quad (4.25)$$

$$\mathbf{E}(\mathbf{V}) = -\rho^{-1} \frac{\partial f^{(0)}}{\partial \mathbf{V}} \xi, \quad (4.26)$$

where

$$\xi = \frac{1}{d} \frac{m_g}{T_g} \int d\mathbf{v} m \mathbf{V} \cdot J_g[f^{(0)}, \mathbf{V} f_g^{(0)}]. \quad (4.27)$$

In Eq. (4.18), we have taken into account that since the production rates ζ and ζ_g are scalar quantities, then their first-order corrections in spatial gradients $\zeta^{(1)}$ and $\zeta_g^{(1)}$ must be proportional to $\nabla \cdot \mathbf{U}$ since ∇n , ∇T , and $\Delta \mathbf{U}$ are vectors and the tensor $\partial_i U_j + \partial_j U_i - \frac{2}{d} \delta_{ij} \nabla \cdot \mathbf{U}$ is traceless. Thus,

$$\zeta^{(1)} = \zeta_U \nabla \cdot \mathbf{U}, \quad \zeta_g^{(1)} = \zeta_{Ug} \nabla \cdot \mathbf{U}, \quad (4.28)$$

where (Garzó 2019)

$$\zeta_U = \frac{\pi^{(d-1)/2}}{2d\Gamma\left(\frac{d+3}{2}\right)} (1 - \alpha^2) \frac{m\sigma^{d-1}}{nT} \int d\mathbf{v}_1 \int d\mathbf{v}_2 f^{(0)}(\mathbf{V}_1) \mathcal{D}(\mathbf{V}_1) g_{12}^3, \quad (4.29)$$

$$\zeta_{Ug} = -\frac{m}{dnT} \int d\mathbf{v} \, V^2 J_g[\mathcal{D}, f_g^{(0)}]. \quad (4.30)$$

The necessary conditions for the solution to the integral equations (4.15)–(4.19) to

exist [Fredholm alternative (Margeneau & Murphy 1956)] is that

$$\int d\mathbf{v} \left\{ 1, \mathbf{v}, \frac{m}{2} V^2 \right\} f^{(1)}(\mathbf{V}) = \{0, \mathbf{0}, 0\}. \quad (4.31)$$

The conditions (4.31) on the first-order distribution $f^{(1)}(\mathbf{V})$ are used later to establish the existence of a unique solution of Eqs. (4.15)–(4.19). The fulfilment of conditions (4.31) necessarily requires that the right sides of the integral equations (4.15)–(4.19) are orthogonal to the set $(1, \mathbf{v}, \frac{m}{2} V^2)$, namely,

$$\int d\mathbf{v} \left\{ 1, \mathbf{v}, \frac{m}{2} V^2 \right\} \begin{pmatrix} \mathbf{A}(\mathbf{V}) \\ \mathbf{B}(\mathbf{V}) \\ C_{ij}(\mathbf{V}) \\ D(\mathbf{V}) \\ \mathbf{E}(\mathbf{V}) \end{pmatrix} = \begin{pmatrix} 0 \\ 0 \\ 0 \\ 0 \\ 0 \end{pmatrix}. \quad (4.32)$$

It is straightforward to prove fulfilment of the conditions (4.32) by direct integration using the definitions (4.22)–(4.26) of \mathbf{A} , \mathbf{B} , C_{ij} , D , and \mathbf{E} , respectively.

4.3. Navier–Stokes transport coefficients

To first order in spatial gradients and based on symmetry considerations, the pressure tensor $P_{ij}^{(1)}$ and the heat flux $\mathbf{q}^{(1)}$ are given, respectively, by

$$P_{ij}^{(1)} = -\eta \left(\frac{\partial U_i}{\partial r_j} + \frac{\partial U_j}{\partial r_i} - \frac{2}{d} \delta_{ij} \nabla \cdot \mathbf{U} \right), \quad (4.33)$$

$$\mathbf{q}^{(1)} = -\kappa \nabla T - \bar{\mu} \nabla n - \kappa_U \Delta \mathbf{U}. \quad (4.34)$$

Here, η is the shear viscosity, κ is the thermal conductivity, $\bar{\mu}$ is the diffusive heat conductivity, and κ_U is the velocity conductivity. To the best of our knowledge, the coefficient κ_U is a new transport coefficient for granular suspensions. This coefficient is also present in driven granular mixtures (Khalil & Garzó 2013, 2018). The Navier–Stokes–Fourier transport coefficients are defined as

$$\eta = -\frac{1}{(d-1)(d+2)} \int d\mathbf{v} R_{ij}(\mathbf{V}) C_{ij}(\mathbf{V}), \quad (4.35)$$

$$\kappa = -\frac{1}{dT} \int d\mathbf{v} \mathbf{S}(\mathbf{V}) \cdot \mathbf{A}(\mathbf{V}), \quad (4.36)$$

$$\bar{\mu} = -\frac{1}{dn} \int d\mathbf{v} \mathbf{S}(\mathbf{V}) \cdot \mathbf{B}(\mathbf{V}), \quad (4.37)$$

$$\kappa_U = -\frac{1}{d} \int d\mathbf{v} \mathbf{S}(\mathbf{V}) \cdot \mathbf{E}(\mathbf{V}). \quad (4.38)$$

In Eqs. (4.35)–(4.38), we have introduced the traceless tensor

$$R_{ij}(\mathbf{V}) = m \left(V_i V_j - \frac{1}{d} V^2 \delta_{ij} \right), \quad (4.39)$$

and the vector

$$\mathbf{S}(\mathbf{V}) = \left(\frac{m}{2} V^2 - \frac{d+2}{2} T \right) \mathbf{V}. \quad (4.40)$$

5. Sonine polynomial approximation to the transport coefficients in steady-state conditions

So far, all the results displayed in section 4 for the transport coefficients η , κ , $\bar{\mu}$, and κ_U are exact. More specifically, their expressions are given by Eqs. (4.35)–(4.38), respectively, where the unknowns \mathcal{A} , \mathcal{B} , \mathcal{C}_{ij} , \mathcal{D} , and \mathcal{E} are the solutions of the integral equations (4.15)–(4.19), respectively. However, it is easy to see that the solution for general *unsteady* conditions requires to solve numerically a set of coupled differential equations for η , κ , $\bar{\mu}$, and κ_U . Thus, in a desire of achieving analytical expressions of the transport coefficients, we consider steady-state conditions. In this case, the constraint $\zeta^{(0)} + \zeta_g^{(0)} = 0$ applies locally and so, the first term of the left-hand side of Eqs. (4.15)–(4.19) vanish. This yields the set of integral equations

$$-\chi \frac{\partial \ln \zeta_g^*}{\partial \chi} \mathcal{A}_i + \mathcal{L} \mathcal{A}_i - \rho^{-1} \frac{\partial f^{(0)}}{\partial V_j} \mathcal{K}_j[\mathcal{A}_i] - J_g[\mathcal{A}_i, f_g^{(0)}] = A_i, \quad (5.1)$$

$$\mathcal{L} \mathcal{B}_i - J_g[\mathcal{B}_i, f_g^{(0)}] - \rho^{-1} \frac{\partial f^{(0)}}{\partial V_j} \mathcal{K}_j[\mathcal{B}_i] = B_i - \varepsilon \frac{\partial \ln \zeta_g^*}{\partial \varepsilon} \mathcal{A}_i, \quad (5.2)$$

$$\mathcal{L} \mathcal{C}_{ij} - \rho^{-1} \frac{\partial f^{(0)}}{\partial V_\ell} \mathcal{K}_\ell[\mathcal{C}_{ij}] - J_g[\mathcal{C}_{ij}, f_g^{(0)}] = C_{ij}, \quad (5.3)$$

$$\mathcal{L} \mathcal{D} - (\zeta_U + \zeta_{Ug}) T \frac{\partial f^{(0)}}{\partial T} - \rho^{-1} \frac{\partial f^{(0)}}{\partial V_i} \mathcal{K}_i[\mathcal{D}] - J_g[\mathcal{D}, f_g^{(0)}] = D, \quad (5.4)$$

$$\mathcal{L} \mathcal{E}_i - \rho^{-1} \frac{\partial f^{(0)}}{\partial V_j} \mathcal{K}_j[\mathcal{E}_i] - J_g[\mathcal{E}_i, f_g^{(0)}] = E_i - \frac{m_g}{T_g} J_g[f^{(0)}, \mathbf{V} f_g^{(0)}]. \quad (5.5)$$

Here, all the quantities appearing in Eqs. (5.1)–(5.5) are evaluated in the steady state.

Apart from considering steady-state conditions, the determination of the explicit forms of the Navier–Stokes–Fourier transport coefficients requires (i) to solve the set of coupled integral equations (5.1)–(5.5) and additionally, (ii) to know the zeroth-order distribution function $f^{(0)}$. Given that both tasks are extremely intricate, one has to consider some approximations.

Regarding the explicit form of $f^{(0)}$, the results obtained in section 3 have shown that the magnitude of the cumulant a_2 is in general very small. Therefore, $f^{(0)}(\mathbf{V})$ can be well represented by the Maxwellian distribution, namely,

$$f^{(0)}(\mathbf{V}) \rightarrow n \left(\frac{m}{2\pi T} \right)^{d/2} \exp \left(- \frac{mV^2}{2T} \right). \quad (5.6)$$

The use of the Maxwellian distribution (5.6) allows us to get simple but accurate expressions for the Navier–Stokes–Fourier transport coefficients. With the Maxwellian approximation (5.6), the collision integral (4.27) can be easily obtained from the results derived by Garzó & Montanero (2007) for arbitrary coefficients of restitution. Particularising to elastic collisions we get

$$\xi = \rho \mu \theta^{-1/2} (1 + \theta)^{1/2} \gamma, \quad (5.7)$$

where

$$\theta = \frac{mT_g}{m_g T} \quad (5.8)$$

is the ratio of the mean square velocities of granular and molecular gas particles. The zeroth-contributions to the production rates are $\zeta^{(0)} = (v_{\text{th}} \zeta^*)/\ell$ and $\zeta_g^{(0)} = (v_{\text{th}} \zeta_g^*)/\ell$,

where

$$\zeta^* = \frac{\sqrt{2}\pi^{(d-1)/2}}{d\Gamma\left(\frac{d}{2}\right)}(1 - \alpha^2), \quad \zeta_g^* = 2x(1 - x^2)\mu^{1/2}\varepsilon, \quad (5.9)$$

and x and ε are defined by Eqs. (3.11) and (3.12), respectively. The Maxwellian approximation to the steady temperature ratio T/T_g can be obtained by inserting the expressions (5.9) of ζ^* and ζ_g^* into the (exact) steady-state condition $\zeta^* + \zeta_g^* = 0$. This yields the cubic equation for x

$$2x(x^2 - 1) = \vartheta, \quad \vartheta = \frac{\sqrt{2}\pi^{(d-1)/2}}{d\Gamma\left(\frac{d}{2}\right)}\mu^{-1/2}\varepsilon^{-1}(1 - \alpha^2). \quad (5.10)$$

The physical root of Eq. (5.10) can be written as (Santos 2003)

$$x = \begin{cases} \frac{\sqrt{3}}{3} \left\{ \sqrt{3} \cos \left[\frac{1}{3} \sin^{-1} \left(\frac{3\sqrt{3}}{4} \vartheta \right) \right] + \sin \left[\frac{1}{3} \sin^{-1} \left(\frac{3\sqrt{3}}{4} \vartheta \right) \right] \right\}, & \vartheta \leq \frac{4\sqrt{3}}{9} \\ \frac{2\sqrt{3}}{3} \cosh \left[\frac{1}{3} \cosh^{-1} \left(\frac{3\sqrt{3}}{4} \vartheta \right) \right], & \vartheta \geq \frac{4\sqrt{3}}{9}. \end{cases} \quad (5.11)$$

According to Eq. (3.11), the temperature ratio T/T_g in the steady state is then given by

$$\frac{T}{T_g} = \frac{m/m_g}{\left(1 + \frac{m}{m_g}\right)x^2 - 1}. \quad (5.12)$$

With respect to the functions $(\mathcal{A}, \mathcal{B}, \mathcal{C}_{ij}, \mathcal{D}, \mathcal{E})$, it is useful to write them in a series expansion of Sonine (Laguerre) polynomials. In practice only the leading terms in these expansions are retained; they provide a quite accurate description over a wide range of inelasticity. In addition, when the cumulants a_2 are neglected, it is straightforward to prove that Eq. (4.25) yields $D = 0$ and so, the production rates $\zeta_U = \zeta_{Ug} = 0$. Non-vanishing contributions to both production rates (which arise from a_2) are expected to be very small (Gómez González & Garzó 2019). Thus, we will focus here our attention in the Navier–Stokes–Fourier transport coefficients η , κ , $\bar{\mu}$, and κ_U defined by Eqs. (4.35)–(4.38), respectively. The procedure for obtaining these transport coefficients is described in the appendix B and only the final expressions in the steady state are provided here.

5.1. Shear viscosity

The shear viscosity coefficient η is given by

$$\eta = \frac{\eta_0}{\nu_\eta^* + K' \tilde{\nu}_\eta \gamma^*}, \quad (5.13)$$

where

$$\eta_0 = \frac{d+2}{8} \frac{\Gamma\left(\frac{d}{2}\right)}{\pi^{(d-1)/2}} \sigma^{1-d} \sqrt{mT} \quad (5.14)$$

is the low density value of the shear viscosity of an ordinary gas of hard spheres ($\alpha = 1$) and

$$K' = \sqrt{2} \frac{(d+2)\Gamma\left(\frac{d}{2}\right)}{8\pi^{(d-1)/2}}. \quad (5.15)$$

Moreover, we have introduced the (reduced) collision frequencies

$$\nu_\eta^* = \frac{3}{4d} \left(1 - \alpha + \frac{2}{3}d\right)(1 + \alpha), \quad (5.16)$$

$$\begin{aligned} \tilde{\nu}_\eta = \frac{1}{(d-1)(d+2)} \left(\frac{m}{m_g} \right)^3 \mu_g \left(\frac{T_g}{T} \right)^2 \theta^{-1/2} & \left\{ 2(d+3)(d-1) (\mu - \mu_g \theta) \theta^{-2} (1+\theta)^{-1/2} \right. \\ & \left. + 2d(d-1) \mu_g \theta^{-2} (1+\theta)^{1/2} + 2(d+2)(d-1) \theta^{-1} (1+\theta)^{-1/2} \right\}, \end{aligned} \quad (5.17)$$

where γ^* is defined in Eq. (3.12). It is important to recall that all the quantities appearing in Eq. (5.13) are evaluated at the steady-state conditions.

5.2. Thermal conductivity, diffusive heat conductivity, and velocity conductivity

We consider here the transport coefficients associated with the heat flux. The thermal conductivity coefficient κ is

$$\kappa = \frac{d-1}{d} \frac{\kappa_0}{\nu_\kappa^* + K' (\tilde{\nu}_\kappa + \beta) \gamma^*}, \quad (5.18)$$

where

$$\kappa_0 = \frac{d(d+2)}{2(d-1)} \frac{\eta_0}{m} \quad (5.19)$$

is the low density value of the thermal conductivity for an ordinary gas of hard spheres and

$$\beta = (x^{-1} - 3x) \mu^{3/2} \left(\frac{T_g}{T} \right)^{1/2}. \quad (5.20)$$

In Eq. (5.18), we have introduced the (reduced) collision frequencies

$$\nu_\kappa^* = \frac{1+\alpha}{d} \left[\frac{d-1}{2} + \frac{3}{16} (d+8)(1-\alpha) \right] (1+\alpha), \quad (5.21)$$

$$\tilde{\nu}_\kappa = \frac{1}{2(d+2)} \mu \frac{\theta}{1+\theta} \left[G - (d+2) \frac{1+\theta}{\theta} F \right], \quad (5.22)$$

where

$$\begin{aligned} F = (d+2)(2\delta+1) + 4(d-1)\mu_g \delta \theta^{-1} (1+\theta) + 3(d+3)\delta^2 \theta^{-1} + (d+3)\mu_g^2 \theta^{-1} (1+\theta)^2 \\ - (d+2)\theta^{-1} (1+\theta), \end{aligned} \quad (5.23)$$

$$\begin{aligned} G = (d+3)\mu_g^2 \theta^{-2} (1+\theta)^2 [d+5+(d+2)\theta] - \mu_g (1+\theta) \left\{ 4(1-d)\delta \theta^{-2} [d+5+(d+2)\theta] \right. \\ \left. - 8(d-1)\theta^{-1} \right\} + 3(d+3)\delta^2 \theta^{-2} [d+5+(d+2)\theta] + 2\delta \theta^{-1} [24+11d+d^2 \\ + (d+2)^2 \theta] + (d+2)\theta^{-1} [d+3+(d+8)\theta] - (d+2)\theta^{-2} (1+\theta) [d+3+(d+2)\theta]. \end{aligned} \quad (5.24)$$

Here, $\delta \equiv \mu - \mu_g \theta$.

The diffusive heat conductivity $\bar{\mu}$ can be written as

$$\bar{\mu} = \frac{K'T}{n} \frac{\kappa_\zeta^*}{\nu_\kappa^* + K' \tilde{\nu}_\kappa \gamma^*}. \quad (5.25)$$

Finally, the velocity conductivity κ_U is given by

$$\kappa_U = -\frac{nT}{2} \frac{K'\mu(1+\theta)^{-1/2} \theta^{-1/2} H}{\nu_\kappa^* + K' \tilde{\nu}_\kappa \gamma^*} \gamma^*, \quad (5.26)$$

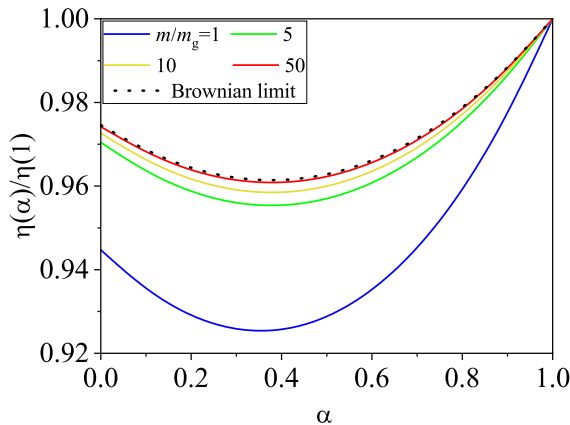


FIGURE 4. Plot of the (scaled) shear viscosity coefficient $\eta(\alpha)/\eta(1)$ versus the coefficient of normal restitution α for $d = 3$, $\phi = 0.001$, $T_g^* = 1000$, and four different values of the mass ratio m/m_g [from top to bottom, $m/m_g = 50, 10, 5$, and 1]. The solid lines are the results derived in this paper while the dotted line is the result obtained by Gómez González & Garzó (2019) by using the suspension model (2.18). Here, $\eta(1)$ refers to the shear viscosity coefficient when collisions between grains are elastic ($\alpha = 1$).

where

$$H = (d+2)(1+2\delta) + 4(1-d)\mu_g(1+\theta)\delta - 3(d+3)\delta^2 - (d+3)\mu_g^2(1+\theta)^2. \quad (5.27)$$

5.3. Brownian limit

Equations (5.13), (5.18), (5.25), and (5.26) provide the expressions of the transport coefficients η , κ , $\bar{\mu}$, and κ_U , respectively, for arbitrary values of the mass ratio m/m_g . As did before in the homogeneous state, it is quite interesting to consider the limiting case $m/m_g \rightarrow \infty$ (Brownian limit). In this limit case, $\mu_g \rightarrow 0$, $\mu \rightarrow 1$, $\chi \equiv \text{finite}$, and so $\theta \rightarrow 0$, $x \rightarrow \chi^{-1/2}$, $\delta \rightarrow 1 - \chi^{-1}$, and $\beta \rightarrow 1 - 3\chi^{-1}$. This yields the results $\tilde{\nu}_\eta \rightarrow 2$ and $\tilde{\nu}_\kappa \rightarrow 3$, so that in the Brownian limit Eqs. (5.13), (5.18), (5.25), and (5.26) reduce to

$$\eta \rightarrow \frac{\eta_0}{\nu_\eta^* + 2K'\gamma^*}, \quad \kappa \rightarrow \frac{d-1}{d} \frac{\kappa_0}{\nu_\kappa^* + K'(\gamma^* - \frac{3}{2}\zeta^*)\gamma^*}, \quad (5.28)$$

$$\bar{\mu} \rightarrow \frac{\kappa T}{n} \frac{K'\zeta^*}{\nu_\kappa^* + 3K'\gamma^*}, \quad \kappa_U \rightarrow 0. \quad (5.29)$$

Equations (5.28) and (5.29) agree with the results obtained by Gómez González & Garzó (2019) by using the suspension model (2.18). This confirms the self-consistency of the results obtained in this paper for general values of the mass ratio.

5.4. Some illustrative systems

In the steady state, the expressions of the Navier–Stokes–Fourier transport coefficients η , κ , $\bar{\mu}$, and κ_U are provided by Eqs. (5.13), (5.18), (5.25), and (5.26), respectively. As in previous works on transport in granular gases (Brey *et al.* 1998; Garzó & Dufty 1999; Garzó *et al.* 2012; Gómez González & Garzó 2019), to highlight the α -dependence of the transport coefficients, they are scaled with respect to their values for elastic collisions. This scaling cannot be made in the case of the diffusive heat conductivity $\bar{\mu}$ since this coefficient vanishes for $\alpha = 1$. In this case, we consider the scaled coefficient $n\bar{\mu}/T\kappa(1)$, where $\kappa(1)$ refers to the value of the thermal conductivity (5.18) for elastic collisions. All these scaled coefficients exhibit a complex dependence on the coefficient of restitution

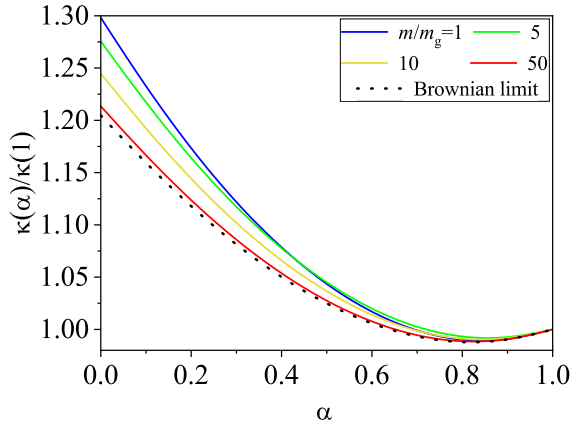


FIGURE 5. Plot of the (scaled) thermal conductivity coefficient $\kappa(\alpha)/\kappa(1)$ versus the coefficient of normal restitution α for $d = 3$, $\phi = 0.001$, $T_g^* = 1000$, and four different values of the mass ratio m/m_g [from top to bottom, $m/m_g = 1, 5, 10$, and 50]. The solid lines are the results derived in this paper while the dotted line is the result obtained by Gómez González & Garzó (2019) by using the suspension model (2.18). Here, $\kappa(1)$ refers to the thermal conductivity coefficient when collisions between grains are elastic ($\alpha = 1$).

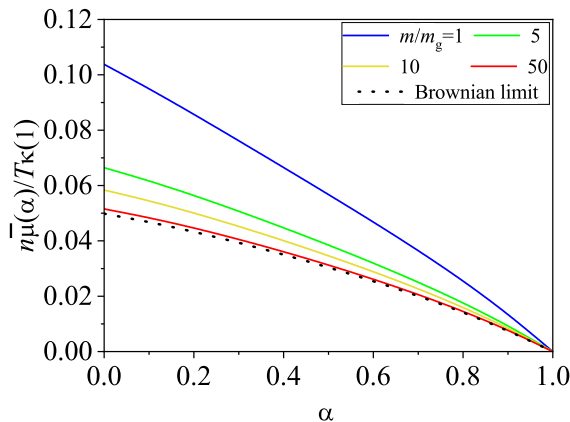


FIGURE 6. Plot of the (scaled) diffusive heat conductivity coefficient $n\bar{\mu}(\alpha)/T\kappa(1)$ versus the coefficient of normal restitution α for $d = 3$, $\phi = 0.001$, $T_g^* = 1000$, and four different values of the mass ratio m/m_g [from top to bottom, $m/m_g = 1, 5, 10$, and 50]. The solid lines are the results derived in this paper while the dotted line is the result obtained by Gómez González & Garzó (2019) by using the suspension model (2.18). Here, $\kappa(1)$ refers to the thermal conductivity coefficient when collisions between grains are elastic ($\alpha = 1$).

α , the mass ratio m/m_g , the volume fraction ϕ [through the parameter ε defined by Eq. (3.12)], and the reduced temperature T_g^* of the molecular gas. Moreover, these dimensionless transport coefficients are defined in terms of the temperature ratio T/T_g , which is given by Eqs. (5.11) and (5.12).

Figures 4–7 show $\eta(\alpha)/\eta(1)$, $\kappa(\alpha)/\kappa(1)$, $n\bar{\mu}/T\kappa(1)$, and $\kappa_U(\alpha)/\kappa_U(1)$, respectively, as functions of the coefficient of restitution α . Here, $\eta(1)$ and $\kappa_U(1)$ correspond to the values of η and κ_U for elastic collisions. Moreover, in the above plots we consider a three-dimensional system ($d = 3$) with $\phi = 0.001$ (very dilute granular gas), $T_g^* = 1000$, and four different values of the mass ratio: $m/m_g = 1, 5, 10$, and 50 . We have also plotted

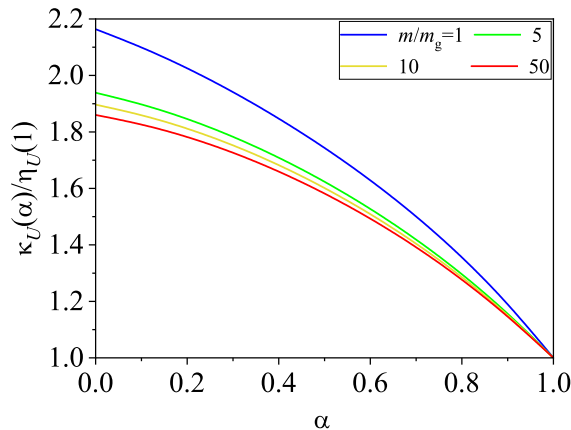


FIGURE 7. Plot of the (scaled) velocity conductivity coefficient $\kappa_U(\alpha)/\kappa_U(1)$ versus the coefficient of normal restitution α for $d = 3$, $\phi = 0.001$, $T_g^* = 1000$, and four different values of the mass ratio m/m_g [from top to bottom, $m/m_g = 1, 5, 10$, and 50]. Here, $\kappa_U(1)$ refers to the velocity conductivity coefficient when collisions between grains are elastic ($\alpha = 1$). Note that in the Brownian limit ($m/m_g \rightarrow \infty$), $\kappa_U \rightarrow 0$, in agreement with the result obtained by Gómez González & Garzó (2019) by using the suspension model (2.18).

the results obtained by Gómez González & Garzó (2019) by using the suspension model (2.18). This model is expected to apply in the Brownian limit ($m \gg m_g$).

We observe that the deviations of the transport coefficients from their elastic forms are in general significant, specially when $m = m_g$. While the (scaled) shear viscosity and thermal conductivity coefficients exhibit a non-monotonic dependence on inelasticity, the (scaled) heat diffusive and velocity conductivity coefficients increase with increasing inelasticity, regardless of the value of the mass ratio considered. In addition, while $\eta(\alpha) < \eta(1)$, the opposite happens for the thermal conductivity since $\kappa(\alpha) > \kappa(1)$. With respect to the dependence on the mass ratio m/m_g , at a fixed value of the coefficient of restitution, it is quite apparent that while the (scaled) shear viscosity increases with increasing the mass ratio, the (scaled) thermal conductivity decreases with increasing the mass ratio. The same happens for the (scaled) coefficients $n\bar{\mu}/T\kappa(1)$ and $\kappa_U(\alpha)/\kappa_U(1)$ since both scaled coefficients decrease as the mass ratio increases. We also see that in the case $m/m_g = 50$, the results derived here for $\eta(\alpha)/\eta(1)$, $\kappa(\alpha)/\kappa(1)$, and $n\bar{\mu}/T\kappa(1)$ practically coincide with those obtained in the Brownian limit by Gómez González & Garzó (2019). However, in the case $m/m_g = 50$, the (scaled) velocity conductivity coefficient $\kappa_U(\alpha)/\kappa_U(1)$ (which vanishes in the Brownian limit) is still clearly different from zero.

Although the results obtained here for the (scaled) transport coefficients depend on the values of the mass ratio and the (reduced) temperature of the molecular gas, it is worthwhile comparing the present results with those obtained for *dry* granular gases (i.e., in the absence of the molecular gas). In the case of the shear viscosity, a comparison between both systems (with and without the gas phase) shows significant discrepancies [see for instance, Fig. 3.1 of the textbook of Garzó (2019)] even at a qualitative level since while η increases with inelasticity for dry granular gases, the opposite happens here whatever the mass ratio considered. On the other hand, a more qualitative agreement is found for the thermal conductivity [see for instance, Fig. 3.2 of Garzó (2019)] since κ increases with decreasing α in both systems. In any case, important quantitative differences appear at strong dissipation since the influence of inelasticity on κ is more relevant in the dry case than in the presence of the molecular gas. A similar conclusion

is reached for the heat diffusive coefficient $\bar{\mu}$ [see for instance, Fig. 3.3 of the textbook of Garzó (2019)] where the magnitude of this (scaled) coefficient for dry granular gases is much more large than the one found here for granular suspensions. In fact, when the particles of the granular gas are much more heavier than those of the molecular gas, given that the magnitude of $n\bar{\mu}/T\kappa(1)$ is much smaller than that of $\kappa(\alpha)/\kappa(1)$ then, one could neglect the contribution coming from the density gradient in the heat flux and assume the validity of Fourier's law $\mathbf{q} = -\kappa\nabla T$.

6. Linear stability analysis of the homogeneous steady state

Once the transport coefficients of the granular gas are known, the corresponding Navier–Stokes hydrodynamic equations can be explicitly displayed. To derive them, one has to take into account first that the the production of momentum $\mathcal{F}[f]$ to first order in spatial gradients can be written as

$$\mathcal{F}^{(1)}[f^{(1)}] = -\xi\Delta\mathbf{U} + \frac{\rho}{d+2}\mu\gamma\left(\frac{\kappa}{n}\frac{\partial\ln T}{\partial r_i} + \frac{\bar{\mu}}{T}\frac{\partial\ln n}{\partial r_i} + \frac{\kappa_U}{nT}\Delta U_i\right)X, \quad (6.1)$$

where ξ is given by Eq. (5.7) and

$$X(\theta) = \theta^{-1/2}(1+\theta)^{-1/2}. \quad (6.2)$$

Thus, when the constitutive equations (4.33)–(4.34) and Eq. (6.1) are substituted into the (exact) balance equations (2.8)–(2.10), one gets the Navier–Stokes hydrodynamic equations for a granular gas immersed in a molecular gas:

$$D_t n + n\nabla \cdot \mathbf{U} = 0, \quad (6.3)$$

$$\begin{aligned} \rho D_t U_i + \frac{\partial p}{\partial r_i} &= \frac{\partial}{\partial r_j} \left[\eta \left(\frac{\partial U_j}{\partial r_i} + \frac{\partial U_i}{\partial r_j} - \frac{2}{d} \delta_{ij} \nabla \cdot \mathbf{U} \right) \right] - \xi \Delta U_i \\ &+ \frac{\rho}{d+2} \mu \gamma X \left(\frac{\kappa}{n} \frac{\partial \ln T}{\partial r_i} + \frac{\bar{\mu}}{T} \frac{\partial \ln n}{\partial r_i} + \frac{\kappa_U}{nT} \Delta U_i \right), \end{aligned} \quad (6.4)$$

$$\begin{aligned} D_t T + T \left(\zeta^{(0)} + \zeta_g^{(0)} \right) &= \frac{2}{dn} \nabla \cdot (\kappa \nabla T + \bar{\mu} \nabla n + \kappa_U \Delta \mathbf{U}) + \frac{2}{dn} \left[\eta \left(\frac{\partial U_j}{\partial r_i} + \frac{\partial U_i}{\partial r_j} \right. \right. \\ &\left. \left. - \frac{2}{d} \delta_{ij} \nabla \cdot \mathbf{U} \right) \frac{\partial U_i}{\partial r_j} - \frac{2}{d} T \nabla \cdot \mathbf{U} \right]. \end{aligned} \quad (6.5)$$

As said in section 5, we have not considered in Eq. (6.5) the first-order contributions to ζ and ζ_g since they vanish when non-Gaussian corrections to the distribution function $f^{(0)}$ are neglected. In addition, as already mentioned in several previous works (Garzó 2005; Garzó *et al.* 2006), the above production rates should also include second-order contributions in spatial gradients. However, in the case of a dry dilute granular gas (Brey *et al.* 1998), it has been shown that these contributions are very small and hence, they can be neglected in the hydrodynamic equations. We expect here that the same happens for a granular suspension. Apart from the above approximations, the Navier–Stokes hydrodynamic equations (6.3)–(6.5) are exact to second order in the spatial gradients of n , \mathbf{U} , and T .

A simple solution of Eqs. (6.3)–(6.5) corresponds to the HSS studied in section 2. A natural question is if actually the HSS may be unstable with respect to long enough wavelength perturbations, as occurs for *dry* granular fluids in freely cooling flows (Goldhirsch & Zanetti 1993; McNamara 1993). This is one of the most characteristic

features of granular gases; its origin is associated with the inelasticity of collisions. On the other hand, the stability of the HSS was also analysed by Gómez González & Garzó (2019) in the Brownian limit case. The results show that the HSS is always linearly stable, in contrast to what happens for dry granular fluids. Since the present work generalises the study carried out by Gómez González & Garzó (2019) to arbitrary values of the mass ratio m/m_g , it is worth to check out if the previous theoretical results (Gómez González & Garzó 2019) are indicative of what occurs when the mass-ratio dependence of the transport coefficients is accounted for. This is the main objective of this section.

As usual, we assume that we slightly perturb the HSS by small spatial gradients and hence, the Navier–Stokes hydrodynamic equations (6.3)–(6.5) are linearised around the HSS. This state describes a homogeneous state ($\nabla n_H = \nabla T_H = 0$) with vanishing flow velocity fields ($\mathbf{U} = \mathbf{U}_g = \mathbf{0}$). In addition, the steady condition is $\zeta_H^{(0)} + \zeta_{gH}^{(0)} = 0$. Here, the subscript H denotes quantities evaluated in the HSS. We suppose that the deviations

$$\delta y_\beta(\mathbf{r}, t) = y_\beta(\mathbf{r}, t) - y_{\beta, H} \quad (6.6)$$

are small. Here, $\delta y_\beta(\mathbf{r}, t)$ denotes the deviations of the hydrodynamic fields

$$\{y_\beta; \beta = 1, \dots, d+2\} \equiv \{n, \mathbf{U}, T\} \quad (6.7)$$

from their values in the homogeneous *steady* state. Moreover, as usual in the simulations of clustering instabilities in fluid-solid systems (Fullmer *et al.* 2017), the molecular gas properties are assumed to be constant and so, they are not perturbed.

Although the reference HSS is stationary [and so, in contrast to what happens in dry granular gases, one does not have to eliminate the time dependence of the transport coefficients through adequate changes of space and time (Brey *et al.* 1998; Garzó 2005)], in order to compare the present stability analysis with the one carried out in the Brownian limit (Gómez González & Garzó 2019), we introduce the following space and time variables:

$$\tau = \frac{v_0}{2\ell} t, \quad \mathbf{r}' = \frac{\mathbf{r}}{2\ell}, \quad (6.8)$$

where $v_0 = \sqrt{T_H/m}$ and $\ell = 1/(n_H \sigma^{d-1})$. The dimensionless time scale τ measures the average number of collisions per particle in the time interval between 0 and t . The unit length \mathbf{r}' is proportional to the mean free path ℓ of solid particles.

The resulting equations for δn , $\delta \mathbf{U}$, and δT can be easily obtained when one substitutes the ansatz (6.6) into Eqs. (6.3)–(6.5) and neglects terms of second and higher order in the perturbations. After some algebra, one gets the set of differential equations:

$$\frac{\partial}{\partial \tau} \frac{\delta n}{n_H} + \nabla' \cdot \frac{\delta \mathbf{U}}{v_0} = 0, \quad (6.9)$$

$$\begin{aligned} \frac{\partial}{\partial \tau} \frac{\delta \mathbf{U}}{v_0} + \nabla' \left(\frac{\delta n}{n_H} + \frac{\delta T}{T_H} \right) &= \frac{d-2}{2d} \eta^* \nabla' \nabla' \cdot \frac{\delta \mathbf{U}}{v_0} + \frac{1}{2} \eta^* \nabla'^2 \frac{\delta \mathbf{U}}{v_0} - 2\xi^* \frac{\delta \mathbf{U}}{v_0} \\ &+ \frac{\sqrt{2}d}{d+2} \mu \gamma^* \left(D_T^* \nabla' \frac{\delta T}{T_H} + \bar{\mu}^* \nabla' \frac{\delta n}{n_H} + 2\kappa_U^* \frac{\delta \mathbf{U}}{v_0} \right) X, \end{aligned} \quad (6.10)$$

$$\begin{aligned} \frac{\partial}{\partial \tau} \frac{\delta T}{T_H} + 2\sqrt{2}\zeta^* \left(\frac{\delta n}{n_H} + \frac{1}{2} \frac{\delta T}{T_H} \right) + 2\sqrt{2}\gamma^* \bar{\zeta}_g \frac{\delta T}{T_H} &= D_T^* \nabla'^2 \frac{\delta T}{T_H} + \bar{\mu}^* \nabla'^2 \frac{\delta n}{n_H} - \left(\frac{2}{d} - 2\kappa_U^* \right) \nabla' \cdot \frac{\delta \mathbf{U}}{v_0}, \end{aligned} \quad (6.11)$$

where $\nabla' \equiv \partial/\partial \mathbf{r}'$ and we have introduced the reduced quantities

$$\eta^* = \frac{\eta_H}{\sigma^{1-d}\sqrt{mT_H}}, \quad \xi^* = \frac{\ell\xi_H}{\rho_H v_0}, \quad D_T^* = \frac{\kappa_H}{d\sigma^{1-d}\sqrt{T_H/m}}, \quad \bar{\mu}^* = \frac{\rho_H \bar{\mu}_H}{d\sigma^{1-d}T_H\sqrt{mT_H}}, \quad (6.12)$$

$$\kappa_U^* = \frac{\kappa_{UH}}{dn_H T_H}, \quad \bar{\zeta}_g = \left(\frac{\mu T_H}{T_g} \right)^{1/2} \left[x_H (1 - x_H^2) - \frac{\mu T_g}{x_H T_H} (1 - 3x_H^2) \right]. \quad (6.13)$$

Here, x_H is defined by Eq. (3.11) with the replacement $T \rightarrow T_H$.

Then, a set of Fourier transformed dimensionless variables are introduced as

$$\rho_{\mathbf{k}}(\tau) = \frac{\delta n_{\mathbf{k}}(\tau)}{n_H}, \quad \mathbf{w}_{\mathbf{k}}(\tau) = \frac{\delta \mathbf{U}_{\mathbf{k}}(\tau)}{v_0}, \quad \theta_{\mathbf{k}}(\tau) = \frac{\delta T_{\mathbf{k}}(\tau)}{T_H}, \quad (6.14)$$

where the elements of the set $\delta y_{\mathbf{k}\beta} \equiv \{\rho_{\mathbf{k}}(\tau), \mathbf{w}_{\mathbf{k}}(\tau), \theta_{\mathbf{k}}(\tau)\}$ are defined as

$$\delta y_{\mathbf{k}\beta}(\tau) = \int d\mathbf{r}' e^{-i\mathbf{k}\cdot\mathbf{r}'} \delta y_{\beta}(\mathbf{r}', \tau). \quad (6.15)$$

Note that here the wave vector \mathbf{k} is dimensionless.

As expected (Brey *et al.* 1998; Garzó 2005), the $d-1$ transverse velocity components $\mathbf{w}_{\mathbf{k}\perp} = \mathbf{w}_{\mathbf{k}} - (\mathbf{w}_{\mathbf{k}} \cdot \hat{\mathbf{k}}) \hat{\mathbf{k}}$ (orthogonal to the wave vector \mathbf{k}) decouple from the other three modes. Their evolution equation is

$$\frac{\partial \mathbf{w}_{\mathbf{k}\perp}}{\partial \tau} + \left(\frac{1}{2} \eta^* k^2 + 2\xi^* - \frac{2\sqrt{2}d}{d+2} \mu \gamma^* \kappa_U^* X \right) \mathbf{w}_{\mathbf{k}\perp} = 0. \quad (6.16)$$

In the Brownian limit ($m/m_g \rightarrow \infty$), $\xi^* = \sqrt{2}\gamma^*$, $X \rightarrow 0$, and Eq. (6.16) is consistent with the one obtained in previous works (Gómez González & Garzó 2019). The solution to Eq. (6.16) is

$$\mathbf{w}_{\mathbf{k}\perp}(\mathbf{k}, \tau) = \mathbf{w}_{\mathbf{k}\perp}(0) \exp[\lambda_{\perp}(k)\tau], \quad \lambda_{\perp}(k) = \frac{2\sqrt{2}d}{d+2} \mu \gamma^* \kappa_U^* X - 2\xi^* - \frac{1}{2} \eta^* k^2. \quad (6.17)$$

A systematic analysis of the dependence of $\lambda_{\perp}(k)$ on the parameter space of the system shows that $\lambda_{\perp}(k)$ is always *negative* and hence, the transversal shear modes $\mathbf{w}_{\mathbf{k}\perp}(\tau)$ are linearly *stable*.

The analysis of the remaining three longitudinal modes ($\rho_{\mathbf{k}}$, $\theta_{\mathbf{k}}$, and the longitudinal velocity component of the velocity field, $w_{\mathbf{k}\parallel} = \mathbf{w}_{\mathbf{k}} \cdot \hat{\mathbf{k}}$) is more intricate since these modes are coupled. In matrix form, they verify the equation

$$\frac{\partial \delta y_{\mathbf{k}\beta}(\tau)}{\partial \tau} + M_{\beta\mu} \delta y_{\mathbf{k}\mu}(\tau) = 0, \quad (6.18)$$

where $\delta y_{\mathbf{k}\beta}(\tau)$ denotes now the set $\{\rho_{\mathbf{k}}, w_{\mathbf{k}\parallel}, \theta_{\mathbf{k}}\}$ and \mathbf{M} is the square matrix

$$\mathbf{M} = \begin{pmatrix} 0 & ik & 0 \\ ik(1 - \sqrt{2}\frac{d}{d+2}\mu\gamma^*\bar{\mu}X) & 2\xi^* - \Theta(k) & ik(1 - \sqrt{2}\frac{d}{d+2}\mu\gamma^*D_T^*X) \\ 2\sqrt{2}\zeta^* + \bar{\mu}^*k^2 & ik(\frac{2}{d} - 2\kappa_U^*) & 2\sqrt{2}(\bar{\zeta}_g\gamma^* + \frac{1}{2}\zeta^*) + D_T^*k^2 \end{pmatrix}, \quad (6.19)$$

where

$$\Theta(k) \equiv \frac{2\sqrt{2}d}{d+2} \mu \gamma^* \kappa_U^* X - \frac{d-1}{d} \eta^* k^2. \quad (6.20)$$

The longitudinal three modes have the form $\exp[\lambda_{\ell}(k)\tau]$ for $\ell = 1, 2, 3$. Here, the

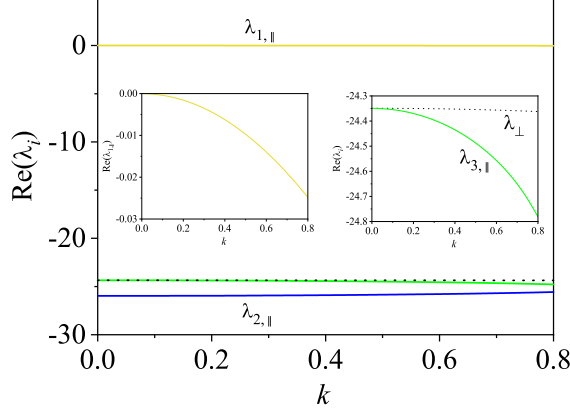


FIGURE 8. Dispersion relations for a three-dimensional granular gas with $\phi = 0.001$, $T_g^* = 1000$, $m/m_g = 1$, and $\alpha = 0.8$. From top to bottom the curves correspond to the longitudinal mode $\lambda_{1,||}$, the two degenerate shear (transversal) modes λ_{\perp} (dotted line) and the two remaining longitudinal modes $\lambda_{3,||}$ and $\lambda_{2,||}$. The dependence of $\lambda_{1,||}$, $\lambda_{3,||}$, and λ_{\perp} on k is shown more clearly in the insets. Only the real parts of the eigenvalues are plotted.

eigenvalues $\lambda_{\ell}(k)$ of the matrix \mathbf{M} are the solutions of the cubic equation

$$\lambda^3 + W(k)\lambda^2 + Y(k)\lambda + Z(k) = 0, \quad (6.21)$$

where

$$W(k) = \sqrt{2} \left(\zeta^* + 2\bar{\zeta}_g \gamma^* + \sqrt{2}\xi^* \right) - \frac{2\sqrt{2}d}{d+2} \mu \gamma^* \kappa_U X + k^2 \left(D_T^* + \frac{d-1}{d} \eta^* \right), \quad (6.22)$$

$$\begin{aligned} Y(k) = \frac{d-1}{d} \eta^* D_T^* k^4 + k^2 \left\{ \frac{2}{d+2} + \sqrt{2} \frac{d-1}{d} (\zeta^* + 2\bar{\zeta}_g \gamma^*) \eta^* - \frac{d}{d+2} \left(\sqrt{2} \mu X \bar{\mu}^* \gamma^* - 1 \right) \right. \\ \left. + \frac{2}{d(d+2)} (d\kappa_U^* - 1) \left[d \left(\sqrt{2} \mu X D_T^* \gamma^* - 1 \right) - 2 \right] + \frac{2}{d+2} D_T^* [(d+2)\xi^* \right. \\ \left. - \sqrt{2} d \mu X \kappa_U^* \gamma^*] \right\} + \frac{2\sqrt{2}}{d+2} (\zeta^* + 2\bar{\zeta}_g \gamma^*) \left[(d+2)\xi^* - \sqrt{2} d \mu X \kappa_U^* \gamma^* \right], \end{aligned} \quad (6.23)$$

$$Z(k) = k^2 \left\{ \sqrt{2} (2\bar{\zeta}_g \gamma^* - \zeta^*) + \frac{2d}{d+2} \mu X \gamma^* \left[2 (\zeta^* D_T^* - \bar{\zeta}_g \bar{\mu}^* \gamma^*) - \zeta^* \bar{\mu}^* \right] + k^2 (D_T^* - \bar{\mu}^*) \right\}. \quad (6.24)$$

In the Brownian limit, Eqs. (6.21)–(6.24) are consistent with those obtained by Gómez González & Garzó (2019).[†]

One of the longitudinal modes $\lambda_{\ell}(k)$ could be unstable for values of the wave number $k < k_h$, where k_h is obtained from Eq. (6.21) when $\lambda = 0$, or equivalently, $Z(k_h) = 0$. This yields the following expressions for k_h :

$$k_h^2 = \frac{\sqrt{2} (2\bar{\zeta}_g \gamma^* - \zeta^*) + \frac{2d}{d+2} \mu X \gamma^* \left[2 (\zeta^* D_T^* - \bar{\zeta}_g \bar{\mu}^* \gamma^*) - \zeta^* \bar{\mu}^* \right]}{\bar{\mu}^* - D_T^*}. \quad (6.25)$$

As in the case of $\lambda_{\perp}(k)$, an study of the dependence of k_h on the parameters of the system

[†] There is a typo in Eq. (99) of Gómez González & Garzó (2019) since the first term of $W(k)$ should be $\sqrt{2} (\zeta^* + 4\chi^{-1} \gamma^* + 2\gamma^*)$.

shows that k_h^2 is always negative. Consequently, there are no physical values of the wave number for which the longitudinal modes become unstable and hence, the longitudinal modes are also linearly *stable*.

In summary, the linear stability analysis of the HSS carried out here for a dilute granular gas surrounded by a molecular gas shows no surprises relative to the earlier study performed in the Brownian limit ($m/m_g \rightarrow \infty$): the HSS is linearly stable for arbitrary values of the mass ratio m/m_g . However, the dispersion relations defining the dependence of the eigenvalues $\lambda_\perp(k)$ and $\lambda_\parallel(k)$ on the parameter space are very different to those previously obtained when $m/m_g \rightarrow \infty$ (Gómez González & Garzó 2019). As an illustration, Fig. 8 shows the real parts of the eigenvalues $\lambda_{i,\parallel}$ ($i = 1, 2, 3$) and λ_\perp as a function of the wave number k for $\phi = 0.001$, $T_g^* = 1000$, $m/m_g = 1$, and $\alpha = 0.8$. It is quite apparent that all the eigenvalues are negative, as expected. In particular, although the longitudinal mode $\lambda_{1,\parallel}$ is quite close to 0, the inset clearly shows that it is always negative. In addition, we also observe that in general the eigenvalues exhibit a very weak dependence on k ; this contrasts with the results obtained for dry granular fluids [see for instance, Fig. 4.7 of Garzó (2019)].

7. Summary and concluding remarks

The main goal of this paper has been to determine the Navier–Stokes–Fourier transport coefficients of a granular gas (modelled as a gas of *inelastic* hard spheres) immersed in a bath of *elastic* hard spheres. We are interested in a situation where the solid particles are sufficiently dilute and hence, one can assume that the state of the molecular gas (bath) is not affected by the presence of grains. Under these conditions, the molecular gas can be considered as a *thermostat* kept at equilibrium at a temperature T_g . This system (granular gas thermostated by a molecular gas) was originally proposed years ago by Biben *et al.* (2002) and it can be considered as a kinetic model for particle-laden suspensions. Thus, in contrast to the previous suspension models employed in the granular literature (Tsao & Koch 1995; Sangani *et al.* 1996; Garzó *et al.* 2012; Saha & Alam 2017) where the effect of the interstitial fluid on grains is accounted for via an effective fluid-solid force, the model considered here takes into account not only the inelastic collisions among grains themselves but also the elastic collisions between particles of the granular and molecular gas. Moreover, we also assume that the volume fraction occupied by the suspended solid particles is very small (low-density regime). In this case, the one-particle velocity distribution function $f(\mathbf{r}, \mathbf{v}; t)$ of grains verifies the Boltzmann kinetic equation.

Before analysing inhomogeneous states, we have considered first homogeneous situations. The study of this state is important because it plays the role of the reference base state in the Chapman–Enskog solution to the Boltzmann equation. In this simple situation, the solid particles are subjected to two competing effects. On the one hand, they collide inelastically so that the granular temperature decreases in time. On the other hand, there is an injection of kinetic energy into the system due to their elastic collisions with the more rapid particles of the molecular gas; this effect tends to thermalise the granular gas to the bath temperature T_g . In the steady state, both competing effects cancel each other and a breakdown of energy equipartition appears ($T < T_g$). In the HSS, the relevant nonequilibrium parameters are the temperature ratio T/T_g and the kurtosis a_2 . This latter quantity measures the deviation of the distribution function from its Gaussian (or Maxwellian) form. Both quantities (T/T_g and a_2) have been here estimated by considering the so-called first Sonine approximation (3.4) to the distribution function $f(\mathbf{v})$. In this approximation, the temperature ratio is obtained by numerically solving Eq.

(3.2) while the kurtosis is given by Eq. (3.26). These equations provide the dependence of T/T_g and a_2 on the parameter space of the system: the mass ratio m/m_g , the (reduced) bath temperature T_g^* [defined by Eq. (3.12)], the volume fraction ϕ [defined by Eq. (3.13)], and the coefficient of restitution α . Our theoretical results extend to arbitrary dimensions the results obtained by Santos (2003) for hard spheres ($d = 3$). To assess the accuracy of the (approximate) analytical results, a suite of Monte Carlo simulations have been also performed. Comparison between theory and simulations shows in general a very good agreement, specially in the case of the temperature ratio.

Once the homogeneous state is characterised, the next step has been to solve the Boltzmann equation by means of the Chapman–Enskog–like expansion (Chapman & Cowling 1970; Brilliantov & Pöschel 2004; Garzó 2019). A subtle point in the expansion is that for small but *arbitrary* perturbations of the HSS, it is expected that the density n and temperature T are specified separately in the *local* reference base state $f^{(0)}(\mathbf{r}, \mathbf{v}; t)$ (zeroth-order approximation). This necessarily implies that the temperature is in general a time-dependent parameter (i.e., $\partial_t^{(0)}T \neq 0$). As mentioned in previous works (Khalil & Garzó 2013; Gómez González & Garzó 2019), this is quite an intricate problem since the complete determination of the transport coefficients in the time-dependent problem requires to solve numerically a set of coupled differential equations. On the other hand, as our main goal is to get the stress tensor and the heat flux to first order in the deviations from the HSS, the corresponding Navier–Stokes–Fourier transport coefficients can be computed to zeroth-order in the deviations from the HSS (steady-state conditions). This simplification allows us to achieve explicit expressions for the above transport coefficients. Their forms are given by Eq. (5.13) for the shear viscosity η , Eq. (5.18) for the thermal conductivity κ , Eq. (5.25) for the diffusive heat conductivity $\bar{\mu}$, and Eq. (5.26) for the so-called velocity conductivity coefficient κ_U . It is quite apparent that the expressions for the scaled coefficients $\eta(\alpha)/\eta(1)$, $\kappa(\alpha)/\kappa(1)$, $n\bar{\mu}(\alpha)/T\kappa(1)$, and $\kappa_U(\alpha)/\kappa_U(1)$ [$\eta(1)$, $\kappa(1)$, and $\kappa_U(1)$ being the values of these coefficients for elastic collisions] show a complex dependence on α , m/m_g , T_g^* , and ϕ . The dependence on the latter two parameters appears via the (reduced) friction coefficient γ^* ; this coefficient provides a characteristic rate for the elastic collisions between granular and bath particles.

Interestingly, in the Brownian limit ($m/m_g \rightarrow \infty$), a careful analysis shows that the expression of η , κ , and $\bar{\mu}$ reduce to those previously derived by Gómez González & Garzó (2019) by using the Langevin-like model (2.18) for the instantaneous gas-solid force. In this limiting case, the coefficient κ_U vanishes. Therefore, the results reported in this paper extend to arbitrary values of the mass ratio m/m_g the resulting transport coefficients for the particle phase derived in previous works (Garzó *et al.* 2012; Gómez González & Garzó 2019).

As expected, we find that in general the impact of the gas phase on the Navier–Stokes–Fourier transport coefficients is non-negligible. In particular, while the (scaled) shear viscosity coefficient $\eta(\alpha)/\eta(1)$ increases with decreasing the coefficient of restitution α for dry (no gas phase) granular gases, Fig. 5 shows clearly that $\eta(\alpha)$ is smaller than $\eta(1)$ in the case of granular suspensions. On the other hand, although a more qualitative agreement on the α -dependence of the (scaled) thermal conductivity coefficient $\kappa(\alpha)/\kappa(1)$ is found for dry granular gases and gas-solid suspensions, significant quantitative differences between both systems appear as the inelasticity in collisions increases. Finally, the differences in the case of the diffusive heat conductivity $\bar{\mu}$ are much more important since the magnitude of the (scaled) coefficient $n\bar{\mu}/T\kappa(1)$ of (dry) granular gases is much more large than that of granular suspensions [see Fig. 7].

The knowledge of the forms of the transport coefficients opens up the possibility of pre-

forming a linear stability analysis on the resulting continuum hydrodynamic equations. As in the Brownian limit case (Gómez González & Garzó 2019), the analysis shows that the HSS is always linearly stable whatever the mass ratio considered is.

One of the main limitations of the results derived in this paper is its restriction to the low-density regime. The extension of the present theory to a moderately dense gas-solid suspension described by the Enskog kinetic equation is an interesting project for the future. These results could stimulate the performance of MD simulations to assess the reliability of the theory for finite densities. Another challenging work could be the determination of the non-Newtonian rheological properties of a granular suspension under simple shear flow. This study would allow to extend previous studies (Tsao & Koch 1995; Sangani *et al.* 1996; Chamorro *et al.* 2015; Saha & Alam 2017; Alam *et al.* 2019; Takada *et al.* 2020) to arbitrary values of the mass ratio m/m_g . Another possible project could be to revisit the results obtained in this paper by considering the charge transport equation recently considered by Ceresiat *et al.* (2021). Work along these lines will be carried out in the near future.

Acknowledgements. The authors acknowledge financial support from Grant PID2020-112936GB-I00 funded by MCIN/AEI/ 10.13039/501100011033, and from Grants IB20079 and GR18079 funded by Junta de Extremadura (Spain) and by ERDF A way of making Europe. The research of R.G.G. also has been supported by the predoctoral fellowship BES-2017-079725 from the Spanish Government.

Declaration of interests. The authors report no conflict of interest.

Author ORCIDs.

Rubén Gómez González: <https://orcid.org/0000-0002-5906-5031>

Vicente Garzó: <https://orcid.org/0000-0001-6531-9328>

Appendix A. First-order distribution function

Some technical details employed in the derivation of the kinetic equation for the first-order distribution $f^{(1)}$ are given in this appendix. To first order in the spatial gradients, the velocity distribution function $f^{(1)}(\mathbf{r}, \mathbf{v}; t)$ verifies the Boltzmann kinetic equation

$$\partial_t^{(0)} f^{(1)} + \mathcal{L} f^{(1)} - J_g[f^{(1)}, f_g^{(0)}] = -\left(D_t^{(1)} + \mathbf{V} \cdot \nabla\right) f^{(0)} - \frac{m_g}{T_g} \Delta \mathbf{U} \cdot J_g[f^{(0)}, \mathbf{V} f_g^{(0)}], \quad (\text{A } 1)$$

where $D_t^{(1)} \equiv \partial_t^{(1)} + \mathbf{U} \cdot \nabla$ and the linear operator \mathcal{L} is defined by Eq. (4.20). To first order, the macroscopic balance equations (2.8)–(2.10) are

$$D_t^{(1)} n = -n \nabla \cdot \mathbf{U}, \quad D_t^{(1)} T = -\frac{2p}{dn} \nabla \cdot \mathbf{U} - T \left(\zeta^{(1)} + \zeta_g^{(1)} \right), \quad (\text{A } 2)$$

$$D_t^{(1)} \mathbf{U} = -\rho^{-1} \nabla p - \xi \Delta \mathbf{U} + \rho^{-1} \mathcal{K}[f^{(1)}], \quad (\text{A } 3)$$

where $\zeta^{(1)}$ and $\zeta_g^{(1)}$ are the first-order contributions to the production rates, the operator $\mathcal{K}[X]$ is defined by Eq. (4.21), and ξ is defined in Eq. (4.27). The production rates are functional of the distribution $f^{(1)}$ and their explicit forms are given by Eqs. (4.28)–(4.30).

The use of the balance equations (A 2) and (A 3) allows one to compute the first term

on the right side of Eq. (A 1). The result is

$$\begin{aligned}
-\left(D_t^{(1)} + \mathbf{V} \cdot \nabla\right) f^{(0)} &= \mathbf{A} \cdot \nabla \ln T + \mathbf{B} \cdot \nabla \ln n + C_{ij} \frac{1}{2} \left(\partial_i U_j + \partial_j U_i - \frac{2}{d} \delta_{ij} \nabla \cdot \mathbf{U} \right) \\
&\quad + D \nabla \cdot \mathbf{U} + \mathbf{E} \cdot \Delta \mathbf{U} + \rho^{-1} \frac{\partial f^{(0)}}{\partial \mathbf{V}} \cdot \boldsymbol{\kappa}[f^{(1)}] \\
&\quad + T \left(\zeta^{(1)} + \zeta_g^{(1)} \right) \frac{\partial f^{(0)}}{\partial T},
\end{aligned} \tag{A 4}$$

where $\partial_i \equiv \partial/\partial r_i$ and the quantities \mathbf{A} , \mathbf{B} , C_{ij} , D , and \mathbf{E} are given by Eqs. (4.22)–(4.26), respectively. Substitution of Eq. (A 4) into Eq. (A 1) yields

$$\begin{aligned}
\partial_t^{(0)} f^{(1)} - T \left(\zeta^{(1)} + \zeta_g^{(1)} \right) \frac{\partial f^{(0)}}{\partial T} &+ \mathcal{L} f^{(1)} - J_g[f^{(1)}, f_g^{(0)}] - \rho^{-1} \frac{\partial f^{(0)}}{\partial \mathbf{V}} \cdot \boldsymbol{\kappa}[f^{(1)}] \\
&= \mathbf{A} \cdot \nabla \ln T + \mathbf{B} \cdot \nabla \ln n + C_{ij} \frac{1}{2} \left(\partial_i U_j + \partial_j U_i - \frac{2}{d} \delta_{ij} \nabla \cdot \mathbf{U} \right) + D \nabla \cdot \mathbf{U} \\
&\quad + \left(\mathbf{E} - \frac{m_g}{T_g} J_g[f^{(0)}, \mathbf{V} f_g^{(0)}] \right) \cdot \Delta \mathbf{U}.
\end{aligned} \tag{A 5}$$

The solution of Eq. (A 5) is of the form

$$\begin{aligned}
f^{(1)}(\mathbf{V}) &= \mathcal{A}(\mathbf{V}) \cdot \nabla \ln T + \mathcal{B}(\mathbf{V}) \cdot \nabla \ln n + C_{ij} \frac{1}{2} \left(\partial_i U_j + \partial_j U_i - \frac{2}{d} \delta_{ij} \nabla \cdot \mathbf{U} \right) \\
&\quad + \mathcal{D}(\mathbf{V}) \nabla \cdot \mathbf{U} + \mathcal{E} \cdot \Delta \mathbf{U}.
\end{aligned} \tag{A 6}$$

Substitution of this into Eq. (A 5) gives the integral equations (4.15)–(4.19). Upon obtaining these equations, we have taken into account that

$$\partial_t^{(0)} \{ \mathcal{A}, \mathcal{B}, C_{ij}, \mathcal{D}, \mathcal{E} \} = - \left(\zeta^{(0)} + \zeta_g^{(0)} \right) T \partial_T \{ \mathcal{A}, \mathcal{B}, C_{ij}, \mathcal{D}, \mathcal{E} \}, \tag{A 7}$$

and the result

$$\begin{aligned}
\partial_t^{(0)} \nabla \ln T &= \nabla \partial_t^{(0)} \ln T = -\nabla \left(\zeta^{(0)} + \zeta_g^{(0)} \right) = - \left[\zeta^{(0)} + \zeta_g^{(0)} \left(1 - \varepsilon \frac{\partial \ln \zeta_g^*}{\partial \varepsilon} \right) \right] \nabla \ln n \\
&\quad - \frac{1}{2} \left[\zeta^{(0)} + \zeta_g^{(0)} \left(1 + 2\chi \frac{\partial \ln \zeta_g^*}{\partial \chi} \right) \right] \nabla \ln T.
\end{aligned} \tag{A 8}$$

Here, ε is defined in Eq. (3.12) and $\chi \equiv T/T_g$.

Appendix B. Leading Sonine approximations to the Navier–Stokes–Fourier transport coefficients

In this appendix, we determine the explicit expressions of the Navier–Stokes–Fourier transport coefficients in steady-state conditions. To obtain them, we consider the leading Sonine approximations to the unknowns \mathcal{A} , \mathcal{B} , C_{ij} , \mathcal{D} , and \mathcal{E} and neglect non-Gaussian corrections to the zeroth-order distribution $f^{(0)}$ (i.e., we take $a_2 = 0$). Since the procedure to obtain these expressions is quite similar to the one employed in some previous works on granular binary mixtures (Garzó & Dufty 2002; Garzó & Montanero 2007), only some partial results will be displayed in this appendix.

B.1. Leading Sonine approximation to η

In the case of the shear viscosity η , the leading Sonine approximation to $\mathcal{C}_{ij}(\mathbf{V})$ (lowest degree polynomial) is

$$\mathcal{C}_{ij}(\mathbf{V}) \rightarrow -f^{(0)}(\mathbf{V})R_{ij}(\mathbf{V})\frac{\eta}{nT^2}, \quad (\text{B } 1)$$

where $f^{(0)}$ is the Maxwellian distribution (5.6) of the granular gas, the polynomial R_{ij} is given by Eq. (4.39), and η is defined in Eq. (4.35). Since $R_{ij}(\mathbf{V})$ is an even polynomial in \mathbf{V} , then $\mathcal{K}_\ell[R_{ij}] = 0$, and the integral equation (5.2) reads

$$-\frac{\eta}{nT^2} \left\{ \mathcal{L}[f^{(0)}\mathcal{R}_{ij}] - J_g[f^{(0)}\mathcal{R}_{ij}, f_g^{(0)}] \right\} = C_{ij}. \quad (\text{B } 2)$$

To determine η , we multiply both sides of Eq. (B 2) by $R_{ij}(\mathbf{V})$ and integrate over velocity. The result can be written as

$$\frac{1}{(d-1)(d+2)} \frac{\eta}{nT^2} \left\{ \int d\mathbf{v} R_{ij}(\mathbf{V}) \mathcal{L} [f^{(0)} R_{ij}] - \int d\mathbf{v} R_{ij}(\mathbf{V}) J_g [f^{(0)} R_{ij}, f_g^{(0)}] \right\} = p. \quad (\text{B } 3)$$

The collision integral involving the linearised Boltzmann collision operator \mathcal{L} is given by (Brey *et al.* 1998)

$$\frac{1}{(d-1)(d+2)} \frac{1}{nT^2} \int d\mathbf{v} R_{ij}(\mathbf{V}) \mathcal{L} [f^{(0)} R_{ij}] = \nu_\eta^* \nu_0, \quad (\text{B } 4)$$

where ν_η^* is defined by Eq. (5.16) and $\nu_0 = p/\eta_0$, η_0 being the shear viscosity of a dilute gas of elastic hard spheres [see Eq. (5.14)]. The collision integral involving the Boltzmann–Lorentz operator J_g can be obtained from previous works on granular mixtures (Garzó & Dufty 2002; Garzó & Montanero 2007) when one particularises to elastic collisions. In terms of the friction coefficient γ , the result is

$$-\frac{1}{(d-1)(d+2)} \frac{1}{nT^2} \int d\mathbf{v} R_{ij}(\mathbf{V}) J_g [f^{(0)} R_{ij}, f_g^{(0)}] = \tilde{\nu}_\eta \gamma, \quad (\text{B } 5)$$

where $\tilde{\nu}_\eta$ is given by Eq. (5.17). The expression (5.13) for η can be easily obtained when one takes into account Eqs. (B 4) and (B 5) in Eq. (B 3).

B.2. Leading Sonine approximation to κ , $\bar{\mu}$, and κ_U

The heat flux transport coefficients κ , $\bar{\mu}$, and κ_U are defined by Eqs. (4.36)–(4.38), respectively. The leading Sonine approximation to \mathcal{A} , \mathcal{B} , and \mathcal{E} is

$$\mathcal{A}(\mathbf{V}) \rightarrow c_\kappa \mathbf{S}(\mathbf{V}) f^{(0)}(\mathbf{V}), \quad \mathcal{B}(\mathbf{V}) \rightarrow c_\mu \mathbf{S}(\mathbf{V}) f^{(0)}(\mathbf{V}), \quad \mathcal{E}(\mathbf{V}) \rightarrow c_{\kappa_U} \mathbf{S}(\mathbf{V}) f^{(0)}(\mathbf{V}), \quad (\text{B } 6)$$

where the Sonine coefficients c_κ , c_μ , and c_{κ_U} are defined, respectively, as

$$\begin{pmatrix} c_\kappa \\ c_\mu \\ c_{\kappa_U} \end{pmatrix} = \frac{2}{d(d+2)} \frac{m}{nT^3} \int d\mathbf{V} \begin{pmatrix} \mathcal{A}(\mathbf{V}) \cdot \mathbf{S}(\mathbf{V}) \\ \mathcal{B}(\mathbf{V}) \cdot \mathbf{S}(\mathbf{V}) \\ \mathcal{E}(\mathbf{V}) \cdot \mathbf{S}(\mathbf{V}) \end{pmatrix} = - \begin{pmatrix} \frac{2}{d+2} \frac{m}{nT^2} \kappa \\ \frac{2}{d+2} \frac{m}{T^3} \bar{\mu} \\ \frac{2}{d+2} \frac{m}{nT^3} \kappa_U \end{pmatrix}. \quad (\text{B } 7)$$

Using the Sonine approximations (B 6), the collision integral (4.21) [when $X = S_i(\mathbf{V})$] is

$$\mathcal{K}_i[S_j] = \int d\mathbf{v} m V_i J_g[S_j f^{(0)}, f_g^{(0)}] = -\delta_{ij} \frac{1}{2} nT^2 \mu \theta^{-1/2} (1 + \theta)^{-1/2} \gamma. \quad (\text{B } 8)$$

Taking into account Eq. (B 8), the integral equation (5.1) becomes

$$-\frac{2}{d+2} \frac{m}{nT^2} \kappa \left\{ -\zeta_g^{(0)} \chi \frac{\partial \ln \zeta_g^*}{\partial \chi} f^{(0)} \mathbf{S} + \mathcal{L}[f^{(0)} \mathbf{S}] - J_g[f^{(0)} \mathbf{S}, f_g^{(0)}] \right\} = \mathbf{A} \\ + \frac{1}{d+2} \frac{\mu\gamma}{n} \theta^{-1/2} (1+\theta)^{-1/2} \frac{\partial f^{(0)}}{\partial \mathbf{V}} \kappa, \quad (\text{B } 9)$$

where use has been made of the Sonine approximation (B 6) to \mathcal{A} . As in the case of the shear viscosity, κ is determined by multiplying both sides of Eq. (B 9) by $\mathbf{S}(\mathbf{V})$ and integrating over \mathbf{V} . After some algebra, one achieves

$$-\zeta_g^{(0)} \chi \frac{\partial \ln \zeta_g^*}{\partial \chi} \kappa + \frac{2}{d(d+2)} \frac{m}{nT^3} \kappa \left\{ \int d\mathbf{V} \mathbf{S} \cdot \mathcal{L}[f^{(0)} \mathbf{S}] - \int d\mathbf{V} \mathbf{S} \cdot J_g[f^{(0)} \mathbf{S}, f_g^{(0)}] \right\} = \frac{d+2}{2} \frac{p}{m}, \quad (\text{B } 10)$$

where we have accounted for the results

$$-\frac{1}{dT} \int d\mathbf{V} \mathbf{S}(\mathbf{V}) \cdot \mathbf{A}(\mathbf{V}) = \frac{d+2}{2m} p, \quad \int d\mathbf{V} \mathbf{S}(\mathbf{V}) \cdot \frac{\partial f^{(0)}}{\partial \mathbf{V}} = 0. \quad (\text{B } 11)$$

The corresponding collision integrals can be written as (Brey *et al.* 1998; Garzó & Dufty 2002; Garzó & Montanero 2007)

$$\frac{2}{d(d+2)} \frac{m}{nT^3} \int d\mathbf{V} \mathbf{S} \cdot \mathcal{L}[f^{(0)} \mathbf{S}] = \nu_\kappa^* \nu_0, \quad (\text{B } 12)$$

$$-\frac{2}{d(d+2)} \frac{m}{nT^3} \int d\mathbf{V} \mathbf{S} \cdot J_g[f^{(0)} \mathbf{S}, f_g^{(0)}] = \tilde{\nu}_\kappa \gamma, \quad (\text{B } 13)$$

where ν_κ^* is defined by Eq. (5.21) while $\tilde{\nu}_\kappa$ is given by Eqs. (5.22)–(5.24). In addition, according to the expression (3.7) of $\tilde{\zeta}_g^{(0)}$, one gets the relation

$$-\zeta_g^{(0)} \chi \frac{\partial \ln \zeta_g^*}{\partial \chi} = \beta \gamma, \quad \beta = (x^{-1} - 3x) \mu^{3/2} \chi^{-1/2}. \quad (\text{B } 14)$$

Substitution of Eqs. (B 12)–(B 14) into Eq. (B 10) leads to the expression (5.18) for κ .

The evaluation of the diffusive heat conductivity $\bar{\mu}$ follows similar steps to those carried out in the evaluation of κ . Taking into account the leading Sonine approximations (B 6) to \mathcal{A} and \mathcal{B} , the integral equation (5.2) reads

$$-\frac{2}{d+2} \frac{m}{T^3} \bar{\mu} \left\{ \mathcal{L}[f^{(0)} \mathbf{S}] - J_g[f^{(0)} \mathbf{S}, f_g^{(0)}] \right\} = \mathbf{B} + \frac{1}{d+2} \frac{\mu\gamma}{T} \theta^{-1/2} (1+\theta)^{-1/2} \frac{\partial f^{(0)}}{\partial \mathbf{V}} \bar{\mu} \\ - \frac{2}{d+2} \frac{m}{nT^2} \zeta_g^{(0)} \kappa f^{(0)} \mathbf{S}, \quad (\text{B } 15)$$

where use has been made of Eq. (B 8) and the result

$$\zeta_g^{(0)} \varepsilon \frac{\partial \ln \zeta_g^*}{\partial \varepsilon} = \zeta_g^{(0)}. \quad (\text{B } 16)$$

Multiplying both sides of Eq. (B 15) by $\mathbf{S}(\mathbf{V})$ and integrating over velocity, one gets

$$(\nu_0 \nu_\kappa^* + \tilde{\nu}_\kappa \gamma) \bar{\mu} = \frac{T}{n} \zeta^{(0)} \kappa, \quad (\text{B } 17)$$

where use has been made of the steady state condition $\zeta_g^{(0)} = -\zeta^{(0)}$. The solution to Eq. (B 17) yields the expression (5.25) for $\bar{\mu}$.

Finally, we consider the coefficient κ_U . As said in the main text, it is a new transport

coefficient not present for dry granular monocomponent gases. Taking into account the expression (5.7) of ξ , Eq. (B8), and the leading Sonine approximation (B6) to \mathcal{E} , the integral equation (5.5) reads

$$-\frac{2}{d+2} \frac{m}{nT^3} \kappa_U \left\{ \mathcal{L}[f^{(0)} \mathbf{S}] - J_g[f^{(0)} \mathbf{S}, f_g^{(0)}] \right\} = -\mu \theta^{-1/2} (1+\theta)^{1/2} \gamma \frac{\partial f^{(0)}}{\partial \mathbf{V}} \\ + \frac{1}{d+2} \frac{\mu \gamma}{nT} \theta^{-1/2} (1+\theta)^{-1/2} \frac{\partial f^{(0)}}{\partial \mathbf{V}} \kappa_U - \frac{m_g}{T_g} J_g[f^{(0)}, \mathbf{V} f_g^{(0)}]. \quad (\text{B } 18)$$

As in the cases of κ and $\bar{\mu}$, one multiplies both sides of Eq. (B8) by $\mathbf{S}(\mathbf{V})$ and integrates over velocity to get

$$(\nu_0 \nu_\kappa^* + \tilde{\nu}_\kappa \gamma) \kappa_U = -\frac{1}{2} nT \mu (1+\theta)^{-1/2} \theta^{-1/2} B \gamma, \quad (\text{B } 19)$$

where use has been made of the result

$$\frac{m_g}{T_g} \int d\mathbf{V} \mathbf{S} \cdot J_g[f^{(0)}, \mathbf{V} f_g^{(0)}] = -\frac{dnT}{2} \mu \gamma (1+\theta)^{-1/2} \theta^{-1/2} B, \quad (\text{B } 20)$$

where the expression of the quantity B is displayed in Eq. (5.27). The expression (5.26) for κ_U can be easily obtained from Eq. (B19).

REFERENCES

- ALAM, M., SAHA, S. & GUPTA, R. 2019 Unified theory for a sheared gas-solid suspension: from rapid granular suspension to its small-Stokes-number limit. *J. Fluid Mech.* **870**, 1175–1193.
- BARRAT, A. & TRIZAC, E. 2002 Lack of energy equipartition in homogeneous heated binary granular mixtures. *Granular Matter* **4**, 57–63.
- BIBEN, T., MARTIN, PH.A. & PIASECKI, J. 2002 Stationary state of thermostated inelastic hard spheres. *Physica A* **310**, 308–324.
- BIRD, G. A. 1994 *Molecular Gas Dynamics and the Direct Simulation Monte Carlo of Gas Flows*. Clarendon, Oxford.
- BOX, G. E. P. & MULLER, MERVIN E. 1958 A note on the generation of random normal deviates. *The Annals of Mathematical Statistics* **29** (2), 610 – 611.
- BREY, J. J., DUFTY, J. W., KIM, C. S. & SANTOS, A. 1998 Hydrodynamics for granular flows at low density. *Phys. Rev. E* **58**, 4638–4653.
- BREY, J. J., DUFTY, J. W. & SANTOS, A. 1999 Kinetic models for granular flow. *J. Stat. Phys.* **97**, 281–322.
- BRILLIANTOV, N. & PÖSCHEL, T. 2004 *Kinetic Theory of Granular Gases*. Oxford University Press, Oxford.
- BRILLIANTOV, N. V. & PÖSCHEL, T. 2006a Breakdown of the Sonine expansion for the velocity distribution of granular gases. *Europhys. Lett.* **74**, 424–430.
- BRILLIANTOV, N. V. & PÖSCHEL, T. 2006b Erratum: Breakdown of the Sonine expansion for the velocity distribution of granular gases. *Europhys. Lett.* **75**, 188.
- CAMPBELL, C. S. 1990 Rapid granular flows. *Annu. Rev. Fluid Mech.* **22**, 57–92.
- CAPECELATRO, J. & DESJARDINS, O. 2013 An Euler–Lagrange strategy for simulating particle-laden flows. *J. Comput. Phys.* **238**, 1.
- CAPECELATRO, J., DESJARDINS, O. & FOX, R. O. 2015 On fluid-particle dynamics in fully developed cluster-induced turbulence. *J. Fluid Mech.* **780**, 578.
- CERESIAT, L., KOLEHMAINEN, J. & OZEL, A. 2021 Charge transport equation for bidisperse collisional granular flows with non-equipartitioned fluctuating kinetic energy. *J. Fluid Mech.* **926**, A35.
- CHAMORRO, M. G., VEGA REYES, F. & GARZÓ, V. 2015 Non-Newtonian hydrodynamics for a dilute granular suspension under uniform shear flow. *Phys. Rev. E* **92**, 052205.

- CHAPMAN, S. & COWLING, T. G. 1970 *The Mathematical Theory of Nonuniform Gases*. Cambridge University Press, Cambridge.
- DAHL, S. R., HRENYA, C. M., GARZÓ, V. & DUFTY, J. W. 2002 Kinetic temperatures for a granular mixture. *Phys. Rev. E* **66**, 041301.
- FERZIGER, J. H. & KAPER, G. H. 1972 *Mathematical Theory of Transport Processes in Gases*. North-Holland, Amsterdam.
- FOX, R. O. 2012 Large-eddy-simulation tools for multiphase flows. *Annu. Rev. Fluid Mech.* **44**, 47.
- FULLMER, W. D. & HRENYA, C. M. 2016 Quantitative assessment of fine-grid kinetic-theory-based predictions. *AIChE* **62**, 11–17.
- FULLMER, W. D. & HRENYA, C. M. 2017 The clustering instability in rapid granular and gas-solid flows. *Annu. Rev. Fluid Mech.* **49**, 485–510.
- FULLMER, W. D., LIU, G., YIN, X. & HRENYA, C. M. 2017 Clustering instabilities in sedimenting fluid-solid systems: critical assessment of kinetic-theory-based predictions using the direct numerical simulation data. *J. Fluid Mech.* **823**, 433.
- GARZÓ, V. 2005 Instabilities in a free granular fluid described by the Enskog equation. *Phys. Rev. E* **72**, 021106.
- GARZÓ, V. 2019 *Granular Gaseous Flows*. Springer Nature, Cham.
- GARZÓ, V., CHAMORRO, M. G. & VEGA REYES, F. 2013 Transport properties for driven granular fluids in situations close to homogeneous steady states. *Phys. Rev. E* **87**, 032201.
- GARZÓ, V. & DUFTY, J. W. 1999 Dense fluid transport for inelastic hard spheres. *Phys. Rev. E* **59**, 5895–5911.
- GARZÓ, V. & DUFTY, J. W. 2002 Hydrodynamics for a granular binary mixture at low density. *Phys. Fluids* **14**, 1476–1490.
- GARZÓ, V., FULLMER, W. D., HRENYA, C. M. & YIN, X. 2016 Transport coefficients of solid particles immersed in a viscous gas. *Phys. Rev. E* **93**, 012905.
- GARZÓ, V. & MONTANERO, J. M. 2007 Navier–Stokes transport coefficients of d -dimensional granular binary mixtures at low-density. *J. Stat. Phys.* **129**, 27–58.
- GARZÓ, V., MONTANERO, J. M. & DUFTY, J. W. 2006 Mass and heat fluxes for a binary granular mixture at low density. *Phys. Fluids* **18**, 083305.
- GARZÓ, V., TENNETI, S., SUBRAMANIAM, S. & HRENYA, C. M. 2012 Enskog kinetic theory for monodisperse gas-solid flows. *J. Fluid Mech.* **712**, 129–168.
- GARZÓ, V., VEGA REYES, F. & MONTANERO, J. M. 2009 Modified Sonine approximation for granular binary mixtures. *J. Fluid Mech.* **623**, 387–411.
- GIDASPOW, D. 1994 *Multiphase Flow and Fluidization*. Academic Press.
- GOLDHIRSCH, I. 2003 Rapid granular flows. *Annu. Rev. Fluid Mech.* **35**, 267–293.
- GOLDHIRSCH, I. & ZANETTI, G. 1993 Clustering instability in dissipative gases. *Phys. Rev. Lett.* **70**, 1619–1622.
- GÓMEZ GONZÁLEZ, R. & GARZÓ, V. 2019 Transport coefficients for granular suspensions at moderate densities. *J. Stat. Mech.* **093204**.
- GÓMEZ GONZÁLEZ, R. & GARZÓ, V. 2020 Non-Newtonian rheology in inertial suspensions of inelastic rough hard spheres under simple shear flow. *Phys. Fluids* **32**, 073315.
- GÓMEZ GONZÁLEZ, R. & GARZÓ, V. 2021 Time-dependent homogeneous states of binary granular suspensions. *Physics of Fluids* **33**, 093315.
- GÓMEZ GONZÁLEZ, R., KHALIL, N. & GARZÓ, V. 2020 Enskog kinetic theory for multicomponent granular suspensions. *Phys. Rev. E* **101**, 012904.
- GÓMEZ GONZÁLEZ, R., KHALIL, N. & GARZÓ, V. 2021 Mpemba-like effect in driven binary mixtures. *Phys. Fluids* **33**, 053301.
- HAYAKAWA, H. & TAKADA, S. 2019 Kinetic theory of discontinuous rheological phase transition for a dilute inertial suspension. *Prog. Theor. Exp. Phys* **083J01**.
- HAYAKAWA, H., TAKADA, S. & GARZÓ, V. 2017 Kinetic theory of shear thickening for a moderately dense gas-solid suspension: From discontinuous thickening to continuous thickening. *Phys. Rev. E* **96**, 042903.
- HEUSSINGER, C. 2013 Shear thickening in granular suspensions: Interparticle friction and dynamically correlated clusters. *Phys. Rev. E* **88**, 050201 (R).
- JACKSON, R. 2000 *The Dynamics of Fluidized Particles*. Cambridge University Press, New York.

- KAWASAKI, T., IKEDA, A. & BERTHIER, L. 2014 Thinning or thickening? Multiple rheological regimes in dense suspensions of soft particles. *EPL* **107**, 28009.
- KHALIL, N. & GARZÓ, V. 2013 Transport coefficients for driven granular mixtures at low-density. *Phys. Rev. E* **88**, 052201.
- KHALIL, N. & GARZÓ, V. 2014 Homogeneous states in driven granular mixtures: Enskog kinetic theory versus molecular dynamics simulations. *J. Chem. Phys.* **140**, 164901.
- KHALIL, N. & GARZÓ, V. 2018 Heat flux of driven granular mixtures at low density: Stability analysis of the homogeneous steady state. *Phys. Rev. E* **97**, 022902.
- KOCH, D. L. 1990 Kinetic theory for a monodisperse gas-solid suspension. *Phys. Fluids A* **2**, 1711–1722.
- KOCH, D. L. & HILL, R. J. 2001 Inertial effects in suspensions and porous-media flows. *Annu. Rev. Fluid Mech.* **33**, 619–647.
- LATTANZI, A. M., TAVANASHAD, V., SUBRAMANIAM, S. & CAPECELATRO, J. 2020 Stochastic models for capturing dispersion in particle-laden flows. *J. Fluid Mech.* **903**, A7.
- LOUGE, M., MASTORAKOS, E. & JENKINS, J. T. 1991 The role of particle collisions in pneumatic transport. *J. Fluid Mech.* **231**, 345–359.
- MARGENEAU, H. & MURPHY, G. M. 1956 *The Mathematics of Physics and Chemistry*. Krieger, Huntington, N.Y.
- MCLENNAN, J. A. 1989 *Introduction to Nonequilibrium Statistical Mechanics*. Prentice-Hall, New Jersey.
- MCMANARA, S. 1993 Hydrodynamic modes of a uniform granular medium. *Phys. Fluids A* **5**, 3056–3069.
- MONTANERO, J. M. & GARZÓ, V. 2002 Monte Carlo simulation of the homogeneous cooling state for a granular mixture. *Granular Matter* **4**, 17–24.
- MONTANERO, J. M. & SANTOS, A. 1997 Simulation of the Enskog equation *à la* Bird. *Phys. Fluids* **9**, 2057–2060.
- MONTANERO, J. M. & SANTOS, A. 2000 Computer simulation of uniformly heated granular fluids. *Granular Matter* **2**, 53–64.
- NANBU, K. 1986 Theoretical basis of the Direct Simulation Monte Carlo method. *15th International Symposium on Rarefied Gas Dynamics* **1**, 369–383.
- VAN NOIJE, T. P. C. & ERNST, M. H. 1998 Velocity distributions in homogeneous granular fluids: the free and heated case. *Granular Matter* **1**, 57–64.
- PARMENTIER, J.-F. & SIMONIN, O. 2012 Transition models from the quenched to ignited states for flows of inertial particles suspended in a simple sheared viscous fluid. *J. Fluid Mech.* **711**, 147–160.
- RADL, S. & SUNDARESAN, S. 2014 A drag model for filtered Euler–Lagrange simulations of clustered gas-particle suspensions. *Chem. Eng. Sci.* **117**, 416–425.
- RAO, K. K. & NOTT, P. R. 2008 *An Introduction to Granular Flow*. Cambridge University Press, Cambridge.
- RÉSIBOIS, P. & DE LEENER, M. 1977 *Classical Kinetic Theory of Fluids*. Wiley, New York.
- RODRÍGUEZ, R. F., SALINAS-RODRÍGUEZ, E. & DUFTY, J. W. 1983 Fokker-Planck and Langevin descriptions of fluctuations in uniform shear flow. *J. Stat. Phys.* **32**, 279–298.
- SAHA, S. & ALAM, M. 2017 Revisiting ignited-quenched transition and the non-Newtonian rheology of a sheared dilute gas-solid suspension. *J. Fluid Mech.* **833**, 206–246.
- SAHA, S. & ALAM, M. 2020 Burnett-order constitutive relations, second moment anisotropy and co-existing states in sheared dense gas-solid suspensions. *J. Fluid Mech.* **887**, A9.
- SANGANI, A. S., MO, G., TSAO, H.-K. & KOCH, D. L. 1996 Simple shear flows of dense gas-solid suspensions at finite Stokes numbers. *J. Fluid Mech.* **313**, 309–341.
- SANTOS, A. 2003 Granular fluid thermostated by a bath of elastic hard spheres. *Phys. Rev. E* **67**, 051101.
- SANTOS, A. & MONTANERO, J. M. 2009 The second and third Sonine coefficients of a freely cooling granular gas revisited. *Granular Matter* **11**, 157–168.
- SARRACINO, A., VILLAMAINA, D., COSTANTINI, G. & PUGLISI, A. 2010 Granular brownian motion. *Journal of Statistical Mechanics: Theory and Experiment* **2010** (04), P04013.
- SETO, R., MARI, R., MORRIS, J. F. & DENN, M. M. 2013 Discontinuous shear thickening of frictional hard-sphere suspensions. *Phys. Rev. Lett.* **111**, 218301.

- SUBRAMANIAM, S. 2020 Multiphase flows: Rich physics, challenging theory, and big simulations. *Phys. Rev. Fluids* **5**, 110520.
- TAKADA, S., HAYAKAWA, H., SANTOS, A. & GARZÓ, V. 2020 Enskog kinetic theory of rheology for a moderately dense inertial suspension. *Phys. Rev. E* **102**, 022907.
- TENNETI, S. & SUBRAMANIAM, S. 2014 Particle-resolved direct numerical simulation for gas-solid flow model development. *Annu. Rev. Fluid Mech.* **46**, 199–230.
- TSAO, H-K & KOCH, D. L. 1995 Simple shear flows of dilute gas-solids. *J. Fluid Mech.* **296**, 211–245.
- WANG, T., GROB, M., ZIPPELIUS, A. & SPERL, M. 2014 Active microrheology of driven granular particles. *Phys. Rev. E* **89**, 042209.
- WYLIE, J. J., ZHANG, Q., LI, YUN & HENGYI, XU 2009 Driven inelastic-particle systems with drag. *Phys. Rev. E* **79**, 031301.